Lateral variation in oxygen fugacity and halogen contents in early Cretaceous magmas in Jiaodong area, East China: Implication for triggers of the destruction of the North China Craton

Xiao-Long Huang [a,*], Peng-Li He [a,b], Xue Wang [a,b], Jun-Wei Zhong [a,c], Yi-Gang Xu [a]

[a] State Key Laboratory of Isotope Geochemistry, Guangzhou Institute of Geochemistry, Chinese Academy of Sciences, Guangzhou 510640, China
[b] University of Chinese Academy of Sciences, Beijing, 100049, China
[c] Faculty of Land Resource Engineering, Kunming University of Science and Technology, Kunming, 650093, China

ARTICLE INFO

ABSTRACT

Pacific subduction has been suggested as the trigger of the destruction of the North China Craton, but evidence for it remains ambiguous. To further investigate this issue, we studied Wulian pyroxene monzonite (123 ± 1 Ma) in the west and Rushan gabbro-diorite (115 ± 1 Ma) in the east of the Sulu orogen, East China. The rocks of both locations are characterized by low TiO_2 but high SiO_2 and K_2O, fractionated REE patterns with notable negative Ta-Nb-Ti anomalies, and by high initial $^{87}Sr/^{86}Sr$ ratios and strongly negative $\varepsilon_{Nd}(t)$ and $\varepsilon_{Hf}(t)$ values. These geochemical and isotopic characteristics can be interpreted to be formed by partial melting of enriched lithosphere mantle refertilized by recycled crustal materials that were associated with the Sulu orogeny. Oxygen fugacities of the Rushan gabbro-diorites, estimated based on magnetite-ilmenite equilibration, are significantly higher than those of Wulian pyroxene monzonite. This lateral difference is mirrored by lower F and F/Cl but higher Cl in biotite in the Rushan gabbro-diorite compared to Wulian pyroxene monzonite. All these data suggest a spatially heterogeneous Cretaceous mantle source in terms of halogens and water contents beneath the Sulu orogen, which was most likely caused by the subduction processes of the Pacific plate. H_2O-rich fluid in the mantle beneath the east of the Sulu orogen closer to the mantle wedge was prominently from early dehydration of subducted slab at shallow depth, while F-bearing fluid to further west was released by dehydrated deeper slab or stagnant oceanic slab within the mantle transition zone.

© 2016 Elsevier B.V. All rights reserved.

1. Introduction

Pacific subduction has been regarded as one of principal triggers of the destruction of the east North China Craton (NCC) (Xu, 2014; Xu et al., 2009; Zhu et al., 2012a, 2012b). Seismic tomography studies revealed a stagnant oceanic slab within the mantle transition zone that extends sub-horizontally westward beneath the East Asian continent to the NNE-trending Daxing'anling-Taihangshan Gravity Lineament (DTGL; Fig. 1a) (Fukao et al., 1992; Zhao et al., 2004). Recycling of these subducted components has been recognized in late Cretaceous and Cenozoic basalts in east China (Sakuyama et al., 2013; Xu, 2014; Xu et al., 2012; Zhang et al., 2009). Thus, the influence of Pacific subduction can be traced back in time at least to late Cretaceous. However, it remains less well assessed as to the role of the Pacific subduction in the destruction of the North China Craton which took place during the Early Cretaceous (Zhu et al., 2012b) or perhaps initiated in Jurassic (Wu et al., 2006).

The destruction of the NCC has been attributed to rapid delamination within the early Cretaceous (e.g., Deng et al., 2007; Gao et al., 2004a; Wu et al., 2005; Xu et al., 2006a, 2006b; Yang et al., 2003, 2005b) or protracted thermo-chemical/mechanical erosion from late Triassic–early Jurassic to late Cretaceous–early Cenozoic (e.g., Li et al., 2014; Menzies and Xu, 1998; Xu, 2001, 2014; Xu et al., 2004a, 2004b, 2009). Basal hydration by subduction-released fluids (Niu, 2005) is also a long-lasting process, which emphasizes the role of water-rich fluids derived from the transition zone (ca. 660 km) associated with the "remote" western Pacific subduction systems (Niu, 2005). The evidence for delamination such as adakitic magmatism or eclogites in the NCC (e.g., Gao et al., 2004a; Gu et al., 2013; Guo et al., 2006; Liu et al., 2009, 2012b; Ma et al., 2013; Wang et al., 2007; Xu et al., 2006a, 2006b; Zhang et al., 2010a, 2010b) is restricted to periphery orogens of the craton (Huang et al., 2012a; Zhai et al., 2007). The destruction of the lithosphere in the southeastern NCC was likely initiated from weakened lithospheric zones such as the Dabie-Sulu orogen and Tan-Lu fault zone along the cratonic margins, and then expanding towards the interiors (Gu et al., 2013; Huang et al., 2012a; Xu et al., 2009). Understanding the nature of lithospheric mantle beneath weakened lithospheric zones is thus
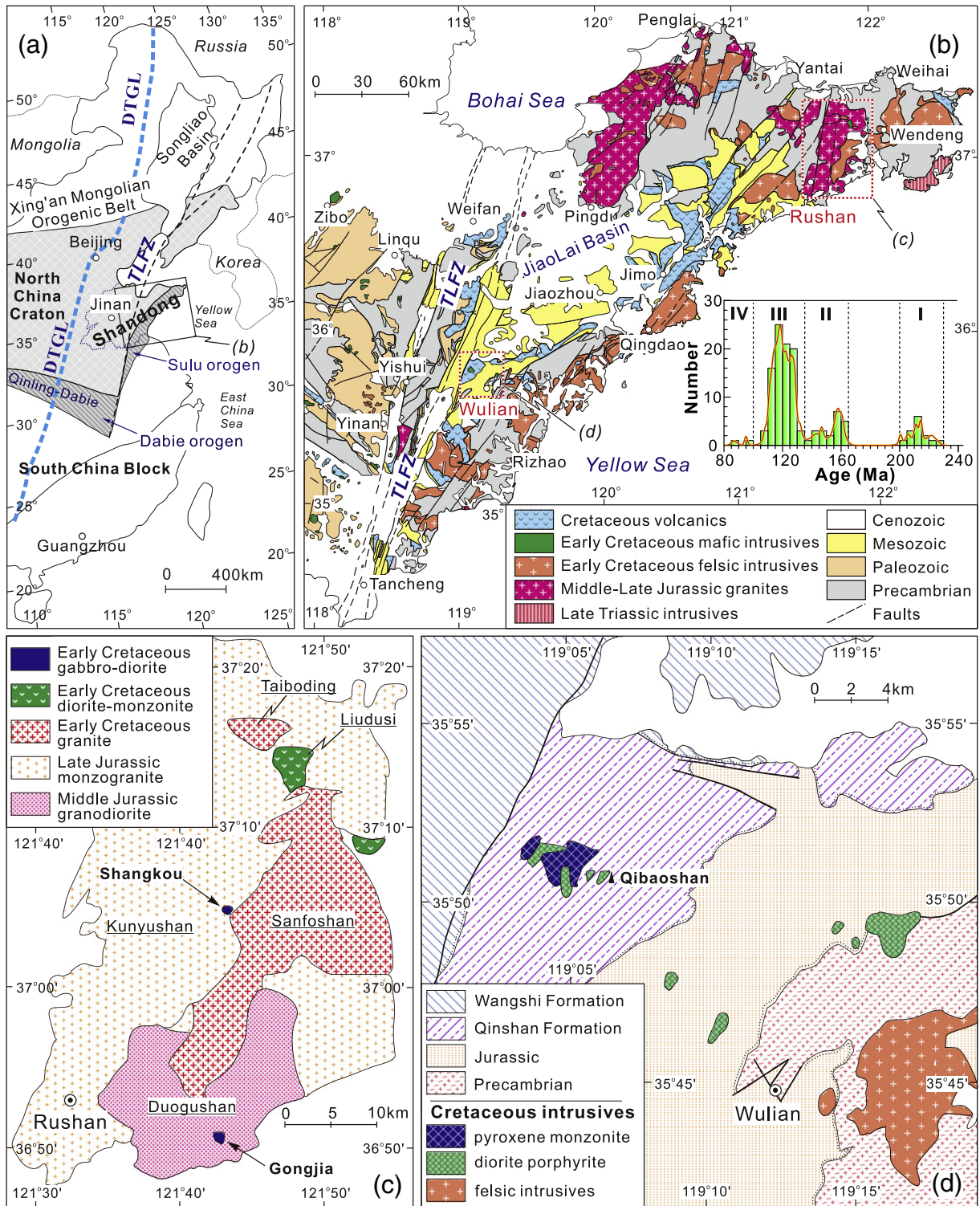
Fig. 1. (a) Simplified tectonic framework in eastern China; the North China Craton is cut by the Tan-Lu fault zone (TLFZ) to the east and the Daxinganling-Taihangshan Gravity Lineament (DTGL) to the west; (b) Distribution of the Mesozoic intrusive and eruptive rocks in Shandong Province and the locations of the Rushan and Wulian mafic intrusions (modified after the geological maps of Shandong Province in 1/1,500,000 scale from the Geological Atlas of China); (c) Geologic sketch map of Rushan area (modified after the Rushan geological map of 1/200,000 scale); (d) Geologic sketch map of the Wulian area (modified after the Rizhao geological map of 1/200,000 scale). The insert geochronology histogram shows the four episodes of Mesozoic magmatism in the Jiaodong Peninsula. Age data are based on the literatures (Cai et al., 2013; Chen et al., 2003; Goss et al., 2010; Guo et al., 2005; Hu et al., 2007; Huang et al., 2006; Li et al., 2012; Liu et al., 2008, 2009, 2011; Liu et al., 2012a, 2012b; Ma et al., 2013, 2014a; Meng et al., 2006; Miao et al., 1997; Qiu et al., 2001; Tang et al., 2009, 2014; Wang et al., 2014; Yang et al., 2005a, 2005b; Zhang and Zhang, 2007; Zhang et al., 2006, 2010b; Zhao et al., 1997; Zhou et al., 2003).

an essential step to gain insight into the processes and mechanism of lithospheric thinning beneath the southeastern NCC.

The Sulu orogen in eastern Shandong witnessed the lithospheric thinning processes in the southeastern NCC for its widespread

magmatism throughout the Mesozoic (Fig. 1b). The geochronology data show four episodes of Mesozoic magmatism (Late Triassic, Late Jurassic, Early Cretaceous and Late Cretaceous) in the Jiaodong Peninsula, and the Early Cretaceous magmatism would be the most

significant according to its wide range of rock types and extensive outcrops (Fig. 1b). However, the petrogenesis of the Early Cretaceous magmatic rocks in the Sulu orogen remains ambiguous, particularly with regard to their source material and geodynamic setting (Tang et al., 2009; Zhang et al., 2010b). These rocks might be ultimately associated with post-orogenic processes subsequent to the collision between the NCC and the Yangtze Craton (e.g., Guo et al., 2004, 2005, 2006; Li et al., 2002; Yang et al., 2005a, 2005b) or the Paleo-Pacific subduction tectonics (Goss et al., 2010; Lan et al., 2011; Ma et al., 2013; Ma et al., 2014a, 2014b). Here we carried out an integrated study on the Early Cretaceous mafic-intermediate intrusions at the Wulian and Rushan locations in the Sulu orogeny (Fig. 1b). With newly acquired zircon U-Pb ages, whole-rock geochemistry and Sr-Nd-Hf isotope data, zircon Lu-Hf isotope data and mineral compositions of biotite and Fe-Ti oxides, we constrain the magma sources involved in petrogenetic processes of the rocks. We show a W-E lateral variation in oxygen fugacity and volatile contents in magma source, which is tentatively related to the subduction of paleo-Pacific plate underneath the eastern Asian continental margin.

2. Geological background and description of samples

The North China Craton (NCC; Fig. 1a), bounded by the Qinling–Dabie–Sulu orogen to the south and the Central Asia orogen to the north, is the oldest and largest cratonic block in China with widespread Archean to Paleoproterozoic basement (e.g., Zhao et al., 2005). The eastern NCC, east of the DTGL, is considered to have encountered tectonothermal remobilization during Phanerozoic time, and was marked by considerable Mesozoic lithospheric thinning (Fan et al., 2000; Gao et al., 2002; Griffin et al., 1998; Menzies and Xu, 1998; Menzies et al., 1993; Xu, 2001, 2007; Zheng et al., 2007). Shandong Province, located in the central part of the eastern NCC, is separated by the left-lateral Tan-Lu fault zone (TLFZ) into two parts (Fig. 1a, b). The western part is the Luxi area where Ordovician diamondiferous kimberlites are situated, and the eastern part is the Jiaodong Peninsula mostly consisting of the Sulu orogen and the Jiaobei terrane (Fig. 1b).

The Sulu orogen formed by the Triassic northward subduction of the Yangtze Craton (YC) beneath the NCC (e.g., Zheng et al., 2003, 2006). The UHP metamorphic rocks in the Sulu orogen are mainly composed of Neoproterozoic granitic gneisses with subordinate coesite-bearing eclogites, schist, and quartzite (Huang et al., 2006; Zheng et al., 2003). Mesozoic igneous rocks in the Sulu orogeny predominantly consist of granitoid rocks with minor mafic rocks (Fig. 1b). Mafic rocks often occur as dikes or small-scale intrusions (Fan et al., 2001; Guo et al., 2004; Meng et al., 2005). The most representative mafic intrusions occur within the Kunyushan suite in the east part and the Qibaoshan intrusive complex in the northwest part of the Sulu orogen (Fig. 1b).

The Kunyushan suite in the Rushan region is composed of the Middle Jurassic granodiorite (Duogushan), Late Jurassic monzogranite (Kunyushan), Early Cretaceous granite (Sanfoshan) and Early Cretaceous gabbro-diorite-monzonite (Fig. 1c). The gabbro-diorite intruded into the Middle Jurassic granodiorite at Gongjia village or the Late Jurassic monzogranite at Shangkou village (Fig. 1c), with total outcrop surface of about 2 km². The studied gabbro-diorite samples collected from a quarry at Gongjia village (Fig. 1c) mainly consist of plagioclase (40–50 %), clinopyroxene (15–25 %) and biotite (5–20 %) with minor orthopyroxene (<3 %), amphibole (<5 %) and Fe-Ti oxides (1–5 %). Accessory minerals include zircon, apatite and titanite. Subhedral-anhedral Fe-Ti oxides occur as inclusions in silicate minerals, especially in clinopyroxene and biotite (Fig. 2a, b). Amphibole is present often around clinopyroxene as the reaction rim (Fig. 2a). Biotite is interstitial to plagioclase and clinopyroxene or as reaction rim around clinopyroxene or Fe-Ti oxides (Fig. 2a, b). Both orthopyroxene and clinopyroxene occur as subhedral-anhedral crystals partially rimed by amphibole or biotite (Fig. 2a, b).

The Qibaoshan intrusive complex in the Wulian region, with outcrop surface of about 12 km², is bounded by the early Creataceous volcanic sequences of Qingshan Formation (Fig. 1d) and comprised of an intrusive association of pyroxene monzonite-dioritic porphyrite. The studied pyroxene monzonite samples consist of clinopyroxene (~10–25 %), plagioclase (~25–40 %), alkali feldspar (~20–35 %) and biotite (~5–15 %) with minor Fe-Ti oxides (1–5 %). Fe-Ti oxides are all anhedral grains enclosed with the silicate minerals, especially pyroxene and biotite (Fig. 2c, d). Biotite occurs as subhedral crystal coexisting with euhedral-subhedral clinopyroxene, or as anhedral interstitial crystal between tabular plagioclases (Fig. 2c, d). Alkali feldspar, present as large anhedral crystal, embeds other silicate minerals such as clinopyroxene, plagioclase and biotite (Fig. 2c, d). Fe-Ti oxides, apatite, zircon and titanite are common accessory minerals in all samples. Fe-Ti oxides in the Rushan and Wulian samples are all intergrowth of ilmenite and magnetite (Fig. 2e, f), with magnetite more abundant in mode than ilmenite.

3. Analytical methods

Zircons were separated using conventional heavy liquid and magnetic techniques and purified by hand-picking under a binocular microscope. They were mounted together with the standard zircons (TEMORA) in epoxy resin. The mount was polished to ensure the exposure of the interiors of the grains and then was gold-coated. Internal structure of zircons was examined using cathodoluminescence (CL) imaging technique prior to U-Pb isotopic analyses. Zircon U-Pb analyses were performed on a CAMECA IMS-1280 ion microprobe at the Institute of Geology and Geophysics, Chinese Academy of Sciences (IGG-CAS) in Beijing, China. Analytical procedures are similar to those described by Li et al. (2009). U-Th-Pb isotopic ratios and absolute abundances were determined relative to the standard zircon 91500 (Wiedenbeck et al., 1995). Measured Pb isotopic compositions were corrected for common Pb using ^{204}Pb signal. Uncertainties on individual analyses are reported at a 1σ level (Supplemental Table 1); data reduction was carried out using Isoplot (ver. 3.23) program (Ludwig, 2003).

Geochemical and Sr-Nd-Hf isotopic analyses were carried out at the Guangzhou Institute of Geochemistry, Chinese Academy of Sciences (GIG-CAS). Samples were sawed into slabs and the central parts (>200 g) were used for bulk-rock analyses. The rocks were crushed into small size (<0.5 cm in diameter) before further cleaned with deionized water in an ultrasonic bath and pulverized in a corundum mill.

Bulk rock major element oxides were analyzed using a Rigaku RIX 2000 X-ray fluorescence spectrometer (XRF). Calibration lines used in quantification were produced by bivariate regression of data from 36 reference materials encompassing a wide range of silicate compositions. Calibrations incorporated matrix corrections based on the empirical Traill-Lachance procedure, and analytical uncertainties are mostly between 1% and 5%. Trace elements were obtained using inductively coupled plasma-mass spectrometry (ICP-MS) after acid digestion of samples in high-pressure Teflon vessels. An internal standard solution containing the single element Rh was used to monitor signal drift. The US Geological Survey and Chinese National standards BCR-1, AGV-2, GSR-1, GSR-2, MRG-1, W-2 and G-2 were chosen for calibrating element concentrations of measured samples. Analytical precision of REE and other incompatible elements of the standard samples is typically 1–5 %. In-run analytical precision for Nd is less 2.5 % RSD (relative standard deviation).

Sr-Nd-Hf isotopic analyses were performed on a subset of whole rock samples using a Neptune Plus multi-collector ICP-MS (MC-ICP-MS). The Sr-Nd isotopic analytical methods follow the analytical procedures described by Li et al. (2006). REE were separated using cation exchange columns, and Nd fractions were further separated by HDEHP-coated Kef columns. Measured $^{143}Nd/^{144}Nd$ ratios were normalized to $^{146}Nd/^{144}Nd = 0.7219$. Reference standards were analyzed
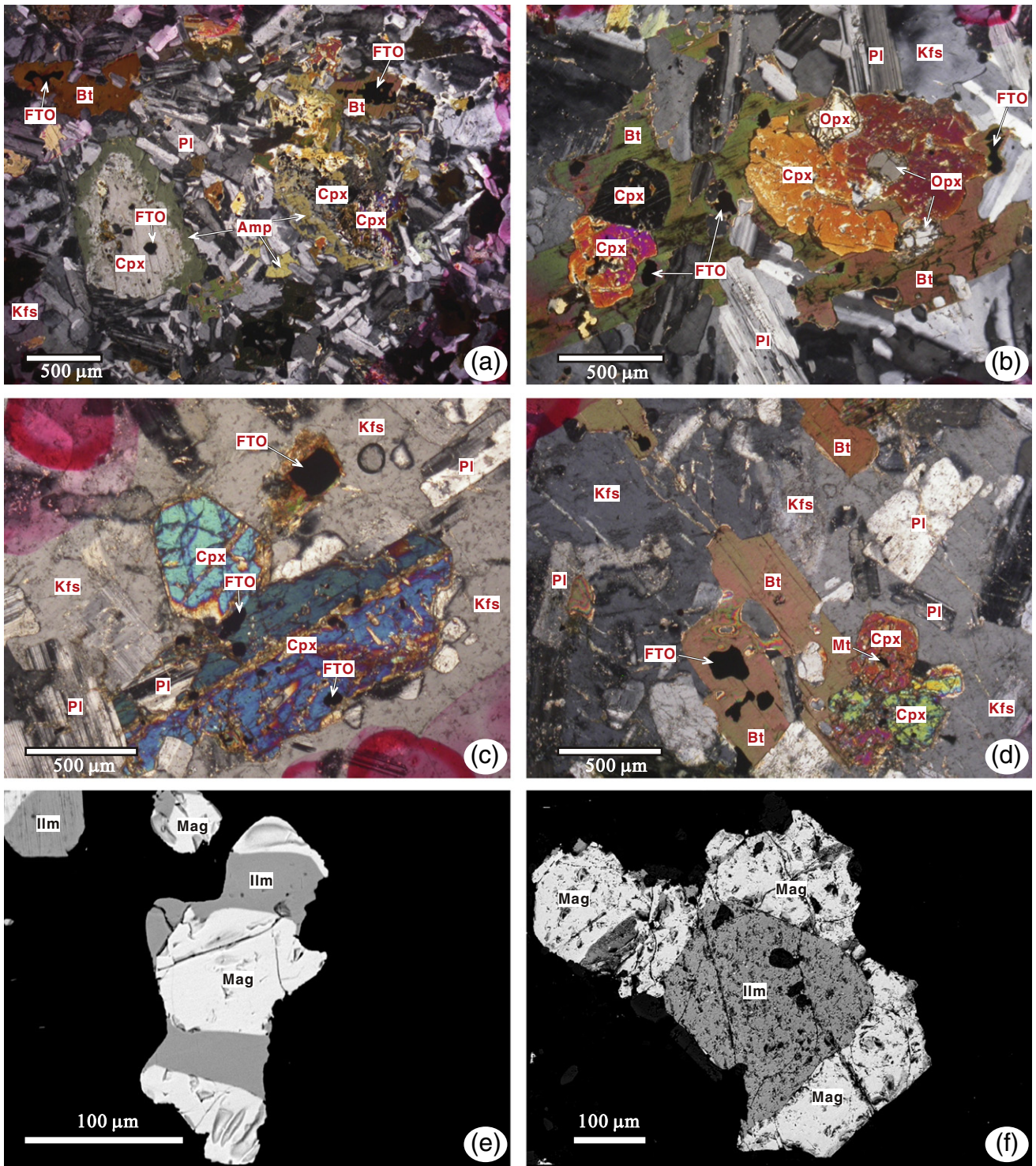
Fig. 2. Petrographic characteristics: (a, b) Rushan porphyry gabbro-diorite, consisting of relatively fine plagioclase (Pl, elongate grains with multiple twinning), alkali feldspar (Kfs), clinopyroxene (Cpx), biotite (Bt), amphibole (Amp), orthopyroxene (Opx) and Fe-Ti oxides (FTO); Amphibole as the reaction rim around clinopyroxene. Biotite (Bt) is interstitial to plagioclase (Pl) and clinopyroxene (Cpx) or as reaction rim around Cpx or Fe-Ti oxides (FTO); (c, d) Wulian pyroxene monzonite, alkali feldspar (Kfs) as large anhedral crystal with inclusions of clinopyroxene (Cpx), plagioclase (Pl), biotite (Bt) and Fe-Ti oxides (FTO); (e) the intergrowth of magnetite (Mag) and ilmenite (Ilm) in the Rushan gabbro-diorite; (f) Fe-Ti oxides in the Wulian pyroxene monzonite (Mag), ilmenite is semi-packed by magnetite (Ilm).

along with samples and gave $^{87}Sr/^{86}Sr = 0.710243 \pm 14$ (2σ, the last 2 digits) for NBS987 and $^{143}Nd/^{144}Nd = 0.512124 \pm 11$ (2σ) for Shin Etsu JNdi-1, which are comparable to the recommended values of NBS987 ($^{87}Sr/^{86}Sr = 0.710248$; McArthur, 1994) and Shin Etsu JNdi-1 ($^{143}Nd/^{144}Nd = 0.512115 \pm 7$; Tannaka et al., 2000).

For Hf isotope analysis, the mixture of about 100 mg rock powder and 200 mg $Li_2B_4O_7$ was fused in a Pt–Au alloy crucible at 1200 °C for

15 minutes in a high-frequency furnace. Quenched piece of alkali glass was dissolved in 2 mol/L HCl. Hf fraction was separated by using a modified single-column Ln extraction chromatography method. Measured $^{176}Hf/^{177}Hf$ ratios were normalized to $^{179}Hf/^{177}Hf = 0.7325$, and reported $^{176}Hf/^{177}Hf$ ratios were further adjusted relative to the standard JMC-475 of 0.282160. Reference standard was analyzed along with samples and give $^{176}Hf/^{177}Hf = 0.282191 \pm 3$ (2σ) for JMC475.

In-situ zircon Hf isotopic analyses were carried out on the dated spots using a Neptune MC-ICPMS, equipped with a 193 nm laser, at the IGG-CAS. Spot sizes of 40 μm with a laser repetition rate of 8 Hz were used, which yielded a typical signal intensity of ~ 5 V at mass ^{180}Hf with the energy density of 15 J/cm^2. The detailed analytical technique and data correction procedures are described in Wu et al. (2006). The mean β_{Yb} (^{172}Yb/^{173}Yb) value obtained from zircon itself was applied for the interference correction of ^{176}Yb and ^{176}Lu on ^{176}Hf (Wu et al., 2006; Xie et al., 2008). ^{176}Yb/^{172}Yb = 0.5886 and ^{176}Lu/^{175}Lu = 0.02655 were used for the elemental fractionation correction (Chu et al., 2002). Due to the extremely low ^{176}Lu/^{177}Hf in zircon (normally < 0.003 in the studied samples; Supplemental Table 2), the isobaric interference of ^{176}Lu on ^{176}Hf is negligible (Iizuka and Hirata, 2005). No relationship between ^{176}Yb/^{177}Hf and ^{176}Hf/^{177}Hf ratios was observed in the studied samples, indicating that the correction of ^{176}Yb interference on ^{176}Hf is precise for obtaining accurate ^{176}Hf/^{177}Hf values. During analysis of the samples, the zircon standard 91500 applied for the instrumental mass fractionation gave ^{176}Hf/^{177}Hf = 0.282292 ± 14 (2σ), which is identical with the ^{176}Hf/^{177}Hf ratios of 0.282284 ± 22 reported by Griffin et al. (2006). The uncertainties of calibrated isotope ratios include those from the sample, standards, and reference values, which are given at ± 2σ in Supplemental Table 2.

Mineral compositions were carried out using a JEOL JXA-8100 Superprobe at the GIG-CAS. The operating conditions are: 15 kV accelerating voltage, 20 nA beam current, 1 − 2 μm beam diameter, and 20 s peak counting time for most elements (60 s for F and Cl, 7 s for Na and 8 s for K in mica, 40 s for Cr, Ti and V in Fe-Ti oxides). The data reduction was done using ZAF correction.

4. Analytical Results

4.1. Zircon U-Pb geochronology and Hf isotopes

The pyroxene monzonite sample WL-15 from Wulian and gabbro sample RS-22 from Rushan were selected for zircon U-Pb dating (Supplemental Table 1) and Lu-Hf isotopic analyses (Supplemental Table 2). The zircon Lu-Hf isotopic analyses were conducted on the same spots that had previously been dated for U-Pb ages using a CAMECA IMS-1280 (Supplemental Table 2). Initial Hf isotope ratios were calculated at their apparent ^{206}Pb/^{238}U ages (Supplemental Table 2). Although zircon grains are entirely of fragments due to over-crushing, their CL images show oscillatory zoning structure (inset in Fig. 3), indicating a magmatic origin.

The zircons of sample WL-15 from Wulian (Fig. 1c) contains moderate to high Th and U contents (170 − 1150 ppm and 167 − 586 ppm, respectively) with high Th/U ratios of 1.01 − 1.96 (Supplemental Table 1). All U-Pb results show a tight grouping of concordant to near concordant apparent ^{206}Pb/^{238}U ages, with a weighted mean value of 123 ± 1 Ma (2σ error; Fig. 2a), reflecting the crystallization age of the Wulian pyroxene monzonite. This age is nearly identical to that of the Shichang-Fangzi monzodiorite-monzogranite complex (122 ± 2 Ma; Yang et al., 2005a) on South Wulian city. Fourteen zircon grains from sample WL-15 have a relatively narrow range of ^{176}Hf/^{177}Hf ratios (0.282276 − 0.282381) that yield negative $\varepsilon_{Hf}(t)$ values (-15.3 to -11.6) (Supplemental Table 2).

The zircons of sample RS-22 from Rushan contain variable Th and U contents (161 − 2221 ppm and 170 − 1609 ppm, respectively) with high Th/U ratios of 0.79 − 1.89 (Supplemental Table 1). All analyses show similar apparent ^{206}Pb/^{238}U ages and yield a weighted mean value of 115 ± 1 Ma (2σ; Fig. 3b), representing the crystallization age of Rushan mafic intrusion. Compared to the data of sample WL-15, the zircons of sample RS-22 have overlapping but broadly slightly lower ^{176}Hf/^{177}Hf ratios (0.282262 − 0.282340) corresponding to negative $\varepsilon_{Hf}(t)$ values from -16.0 to -13.3 (Supplemental Table 2).
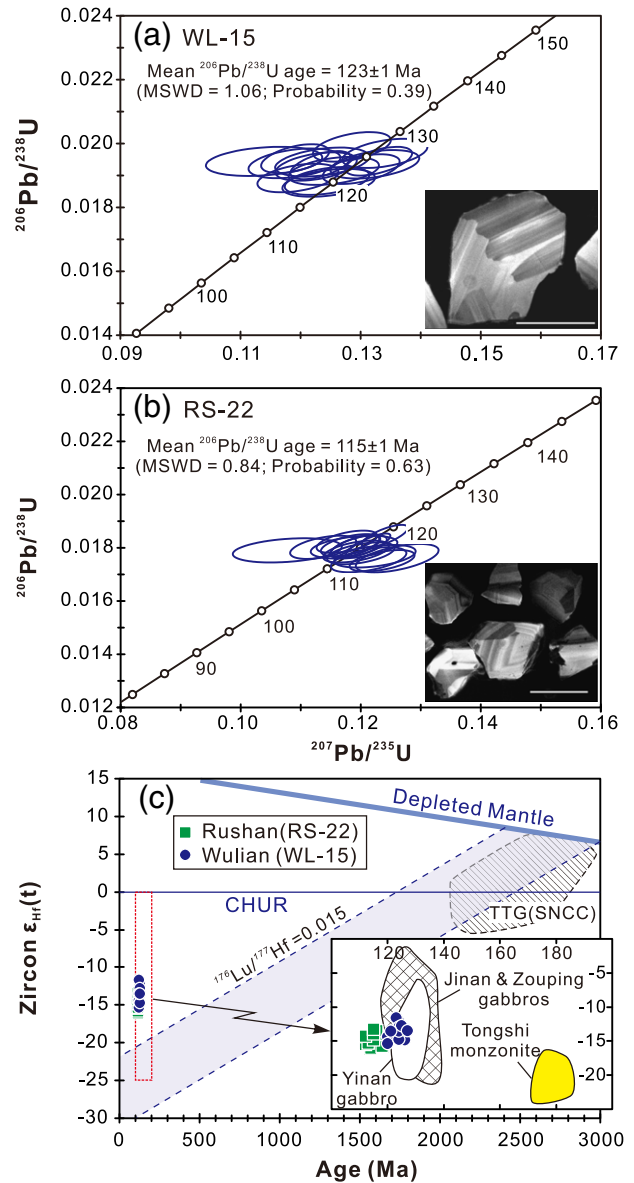

Fig. 3. (a, b) Concordia diagrams for SIMS zircon U-Pb chronology of the Wulian and Rushan mafic intrusive rocks. MSWD and Probability of concordance are at the 1σ level. The scale bar of CL images is 100 μm. (c) Plot of zircon $\varepsilon_{Hf}(t)$ vs. age of the Wulian and Rushan mafic intrusions; ages are apparent ^{206}Pb/^{238}U ages by U-Pb dating; the evolution of depleted mantle (DM) is drawn using a present-day ^{176}Hf/^{177}Hf = 0.28325 and ^{176}Lu/^{177}Hf = 0.0384 (Griffin et al., 2000); the fields of Mesozoic intrusions in western Shandong Province (Tongshi, Yinan and Jinan-Zouping areas) are after Huang et al. (2012a); the field of the TTG in the southern North China Craton (SNCC) is compiled from the data in Huang et al. (2010, 2012b, 2013).

4.2. Major and trace elements

Bulk rock analyses of 16 samples are presented in Supplemental Table 3 and plotted in Fig. 4, which include seven gabbro-diorite samples from Rushan and nine pyroxene monzonite samples from Wulian.

The Rushan gabbro-diorite samples have variable SiO$_2$ (53.48 − 59.58 wt%), MgO (2.61 − 5.50 wt%), Fe$_2$O$_3$ (6.10 − 8.38 wt%), CaO (4.64 − 7.66 wt%), high Na$_2$O (3.70 − 4.18 wt%) and K$_2$O (2.71 − 3.85 wt%) with low TiO$_2$ (0.85 − 1.08 wt%). The major elements of studied samples are comparable with the literature data of the gabbro-diorite from the same locality (Hu et al., 2007; Meng et al., 2005; Tang et al., 2009) (Fig. 4). The samples have fractionated REE patterns ([La/Yb]$_N$ = 22.3 − 30.1; Supplemental Table 3) with weak negative Eu anomalies (Eu/Eu* = 0.77 − 0.92; Supplemental Table 3)
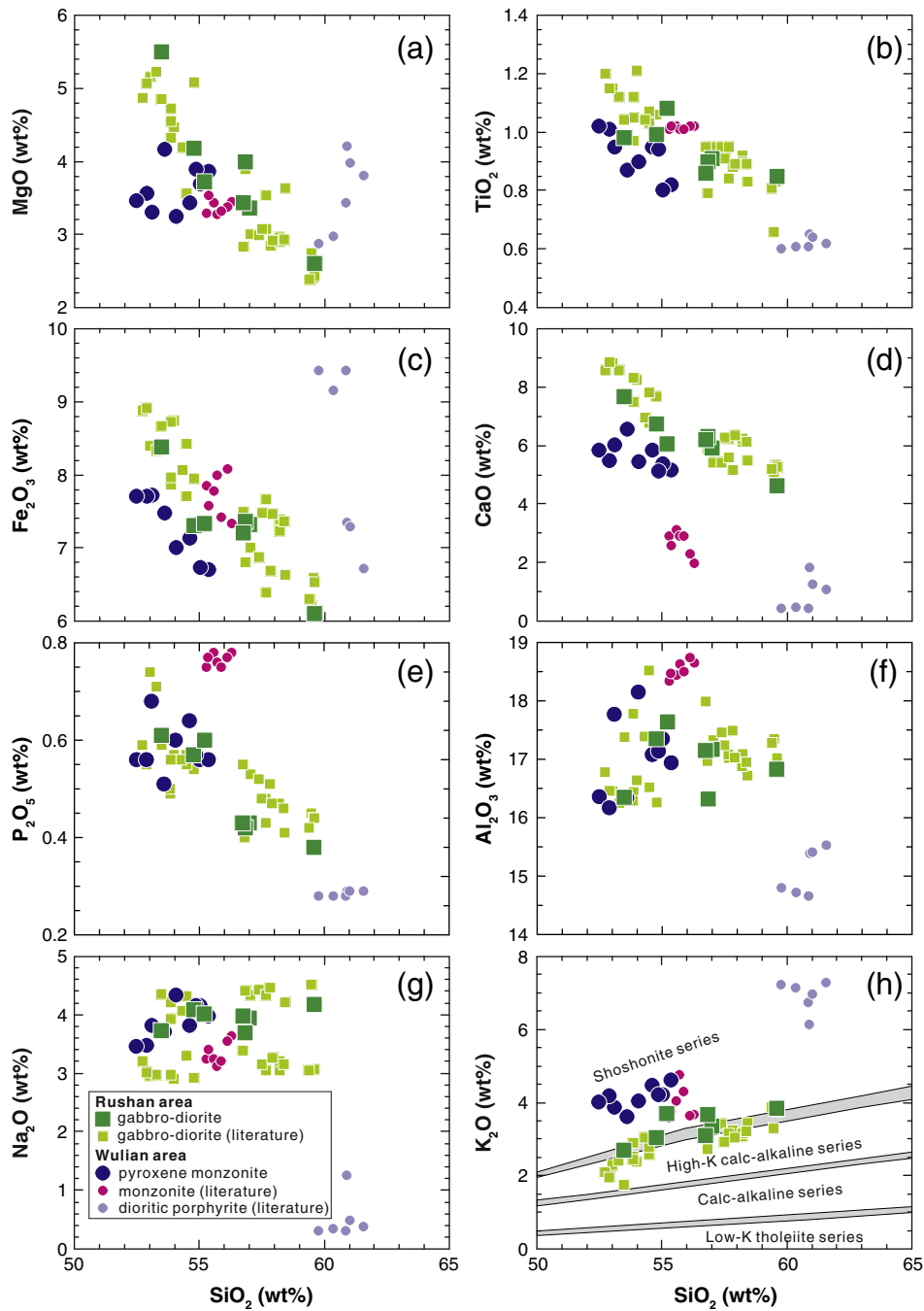
Fig. 4. SiO₂ variation diagrams of representative major element oxides and minor elements for the Wulian and Rushan mafic intrusions. The literature data of Rushan gabbro-diorite (Hu et al., 2007; Meng et al., 2005; Tang et al., 2009), Wulian pyroxene monzonites and dioritic porphyrites (Liu et al., 2009, 2011) are shown for comparison.

(Fig. 5a), and are characterized by pronounced negative Nb-Ta and Ti anomalies and positive Sr and Pb anomalies in the primitive mantle-normalized multi-element diagram (Fig. 5b).

The Wulian pyroxene monzonite samples have relatively narrow ranges of SiO₂ (52.48 — 55.36 wt%), MgO (3.25 — 4.17 wt%), Fe₂O₃ (6.70 — 7.70 wt%), CaO (5.13 — 6.57 wt%) and K₂O (3.62 — 4.62 wt%) with low TiO₂ (0.80 — 1.02 wt%). These pyroxene monzonite samples have higher CaO, MgO and Na₂O but lower SiO₂ than the data of the Wulian monzonite reported in Liu et al. (2009, 2011) (Fig. 4). Overall, the Wulian pyroxene monzonite and dioritic porphyrite have much higher K₂O but lower CaO than the Rushan mafic-intermediate intrusion (Fig. 4d, f). The Wulian samples also show fractionated REE patterns ([La/Yb]$_N$ = 50.3 — 74.9; Supplemental Table 3) with moderate negative Eu anomalies (Eu/Eu* = 0.62 — 0.85; Supplemental

Table 3) (Fig. 5a). In the primitive mantle-normalized multi-element diagram (Fig. 5b), the Wulian samples all exhibit pronounced negative Nb-Ta-Ti anomalies and positive Sr and Pb anomalies. They have overall higher Ba, Th, U, K, Pb, Sr, Zr, Hf and LREE than the Rushan samples (Fig. 5).

4.3. Bulk-rock Sr-Nd-Hf Isotopes

The Rushan gabbro-diorites have high initial ⁸⁷Sr/⁸⁶Sr ratios (0.7075 — 0.7082) and variable negative ε$_{Nd}$(t) (-12.9 to -7.6) (Supplemental Table 4). The Wulian pyroxene monzonites have more negative ε$_{Nd}$(t) (-15.0 to -13.7) than the Rushan gabbro-diorites in similar initial ⁸⁷Sr/⁸⁶Sr ratios of 0.7078 — 0.7082 (Supplemental Table 4). The depleted mantle Nd model ages (T$_{DM}$) of the Rushan gabbro-diorites
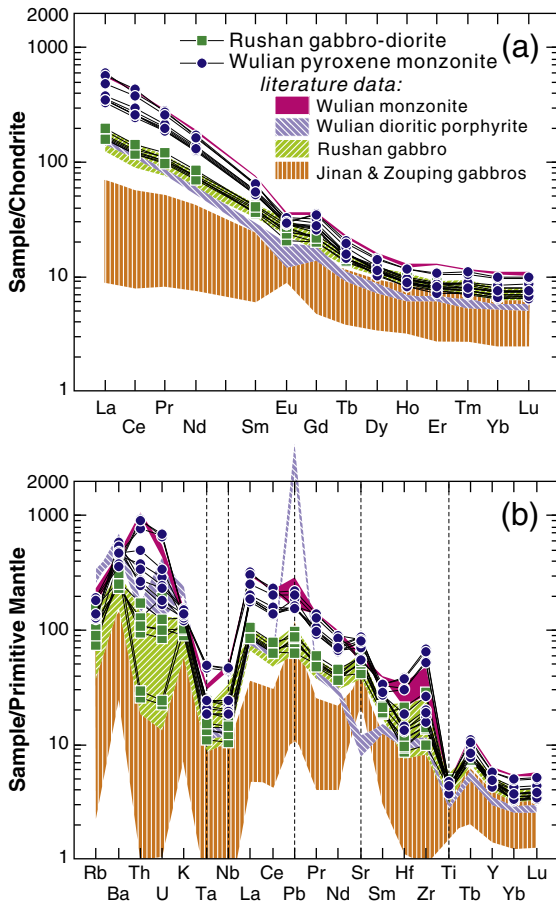
Fig. 5. Chondrite-normalized REE patterns and primitive mantle-normalized trace element spidergrams for the Wulian and Rushan mafic intrusions. The literature data of Rushan gabbro-diorite (Hu et al., 2007; Meng et al., 2005; Tang et al., 2009), Wulian pyroxene monzonites and dioritic porphyrites (Liu et al., 2009, 2011) and Jinan-Zouping gabbros (Huang et al., 2012a) are shown for comparison. Chondrite and PM normalization factors are from Taylor and McLennan (1985) and Sun and McDonough (1989), respectively.
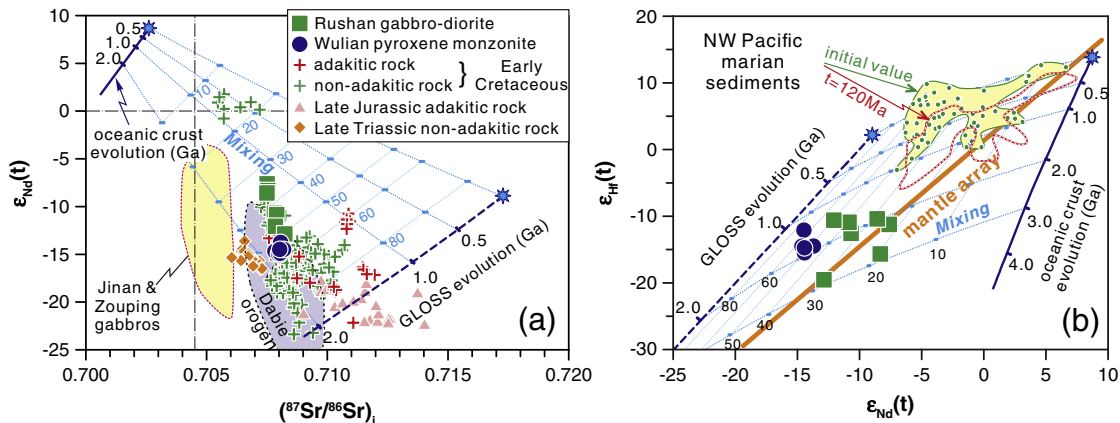
vary from 1.34 Ga to 1.58 Ga (Supplemental Table 4), whereas the Wulian pyroxene monzonites samples have similar Nd model ages (T_{DM} = 1.47–1.58 Ga; Supplemental Table 4). Initial $^{87}Sr/^{86}Sr$ ratios of the Wulian and Rushan rocks are much higher than those of the Early Cretaceous gabbros in the Jinan region (Fig. 6), located to the west of the TLFZ (Fig. 1a).

The Wulian pyroxene monzonite samples have negative $\varepsilon_{Hf}(t)$ values clustered around -15.5 to -12.1, whereas the Rushan gabbro-diorite samples have more variable $\varepsilon_{Hf}(t)$ values from -19.4 to -8.7 (Supplemental Table 4). The Nd-Hf isotopic compositions for the Rushan samples scatter along the mantle array line (Chauvel et al., 2008), while the Wulian samples plot all above the array line (Fig. 6b). Following Chauvel et al. (2008), we calculate the $\Delta\varepsilon_{Hf}$ values (the difference in ε_{Hf} relative to the ε_{Nd}–ε_{Hf} mantle array, defined as $\Delta\varepsilon_{Hf} = \varepsilon_{Hf} - 1.59\varepsilon_{Nd} - 1.28$) to evaluate the degree of Nd–Hf decoupling of the Wulian and Rushan rocks. The Rushan samples exhibit variable $\Delta\varepsilon_{Hf}$ values from -3.6 to +9.2, while the Wulian samples have overall higher $\Delta\varepsilon_{Hf}$ values from +6.0 to +9.7 (Supplemental Table 4)

4.4. Mineral compositions

Biotites in the Rushan gabbro-diorite, Wulian pyroxene monzonite and Jinan gabbro are compositionally heterogeneous within sample (Supplemental Table 5; Fig. 7). The biotites in the Rushan samples have lower MgO, TiO$_2$ and F concentrations, F/Cl ratios and Mg$^{\#}$ values but higher FeO, MnO and Cl than those in the Wulian samples and Jinan gabbro (Fig. 7). The biotites in the Wulian samples contain wide range of fluorine (up to 1.81 wt%; Table 5) with wide range of F/Cl ratios (Fig. 7a, b). For all data from the Rushan and Wulian samples, there is a pronounced negative correlation between MgO and FeO^T (Fig. 7e) and a weak positive correlation between Mg$^{\#}$ and fluorine (Fig. 7d).

The pairs of intergrown ilmenite and magnetite (Fig. 2e, f) were examined for the estimation of oxygen fugacity (Supplemental Table 6 and Fig. 8). For comparison, we also measured those from the Jinan gabbro in the interior of the NCC (Huang et al., 2012a) and the Tekesi gabbro associated with the Tarim plume in the Southwest Tianshan orogen, NW China (He et al., 2013). Magnetite in the Wulian samples is titanomagnetite with Fe^{3+}/Fe^{2+} ratios from 1.31 to 1.59 and TiO$_2$ from 3.31 to 7.13 wt% (Supplemental Table 6; Fig. 8). By contrast,

Fig. 6. (a) Initial $\varepsilon_{Nd}(t)$ vs. $^{87}Sr/^{86}Sr$ and (b) $\varepsilon_{Nd}(t)$ vs. $\varepsilon_{Hf}(t)$ for the Wulian and Rushan mafic intrusions. The Mesozoic igneous rocks in Jiaodong area shown for comparison are based on the literatures (Cai et al., 2013; Gao et al., 2004b; Guo et al., 2004; Hou et al., 2007; Hu et al., 2005, 2007; Lan et al., 2011; Li et al., 2012; Liu et al., 2008, 2009, 2011, 2012a; Ma et al., 2013, 2014a, 2014b; Meng et al., 2006; Tang et al., 2009, 2014; Yang et al., 2003, 2005a, 2005b; Zhang et al., 2010a, 2010b). The fields of the Jinan-Zouping gabbro-diorites and the Mesozoic metamorphic and igneous rocks in the Dabie orogenic belt are after Huang et al. (2012a). NW China marine sediment data are from Vervoort et al. (2011). The present-day average Nd-Hf isotopic compositions of oceanic crust (Chauvel et al., 2008) and Global Subducted Sediment (GLOSS) (Plank and Langmuir, 1998) are also shown in the diagrams. The evolution paths of oceanic crust and GLOSS are shown as dotted and dashed curves, respectively, marked by ages (Ga). To calculate the initial isotope ratios of oceanic crust and GLOSS at different times in the Earth's history, we assumed: they were formed by similar processes and recycled into the mantle at the same time; there is a linear relationship between their isotopic ratios at present and 4.55 Ga. Mixing curves between GLOSS and oceanic crust were marked by the GLOSS proportions in percentage.
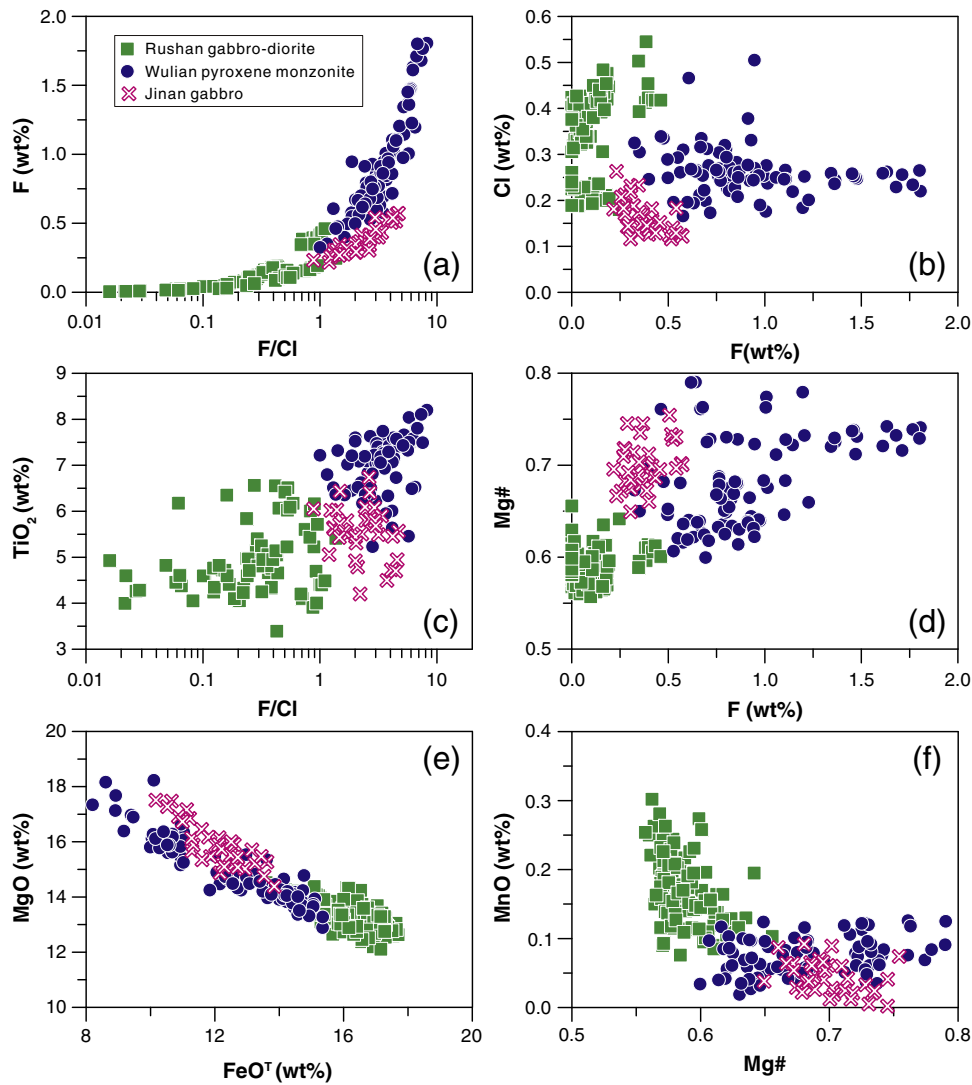
Fig. 7. Plots of (a) F vs. F/Cl; (b) Cl vs. F; (c) TiO_2 vs. F/Cl; (d) $Mg^{\#}$ vs. F; (e) MgO vs. FeO^T; and (f) MnO vs. $Mg^{\#}$ for the biotites from Rushan gabbro-diorite and Wulian pyroxene monzonite. The data of Jinan gabbros in the western Shangdong are shown for comparison.

magnetite in the Rushan samples contains extremely low TiO_2 with high Fe^{3+}/Fe^{2+} ratios close to 2 (Fig. 8a). There is a negative correlation between TiO_2 and Fe^{3+}/Fe^{2+} of all magnetites (Fig. 8a). Ilmenite in the Wulian samples also has relatively higher TiO_2 but lower Fe^{3+}/Fe^{2+} ratio than that in the Rushan samples, defining a negative correlation between TiO_2 and Fe^{3+}/Fe^{2+} (Fig. 8b). Oxygen fugacity and temperature of Fe–Ti oxide crystallization were estimated using the ilmenite–magnetite geothermobarometry program (ILMAT120; Lepage, 2003). Calculated temperature and oxygen fugacity ($\log fO_2$) are listed in Supplemental Table 4 and plotted in a temperature vs. $\log fO_2$ diagram (Fig. 8c), which shows that Fe-Ti oxides of the Wulian samples were formed in relatively lower oxygen fugacity but higher temperature in comparison with those of the Rushan samples (Fig. 8c). Overall, the Fe-Ti oxides of the Wulian samples are similar to those of the Jinan and Tekesi gabbros (Fig. 8).

5. Discussion

5.1. Petrogenesis of the Wulian and Rushan mafic-intermediate complexes

5.1.1. Fractional crystallization

The Wulian pyroxene monzonites exhibit almost uniform Sr-Nd-Hf isotopes (Fig. 6), indicating that variable concentrations of major and

trace elements (Figs. 5, 6) would be primarily attributed to varying degrees of fractional crystallization. The low Cr, Co, Ni and MgO but high SiO_2 and Al_2O_3 of the Wulian pyroxene monzonites (Supplemental Table 3) suggest extensive fractionation of mafic minerals in the early magma stage. However, for narrow ranges of CaO, MgO, Cr, Co and Ni (Figs. 4, 9), olivine or clinopyroxene fractional crystallization would not be a primary process inducing geochemical variation within the Wulian samples. The negative Eu anomalies of the REE patterns (Fig. 5a) and positive correlations between Eu/Eu* and Sr/Sr* ($=2 \times Sr_{PM}/[Sm_{PM} + Nd_{PM}]$), Sr/Y or Ba (Fig. 9d, e, f) indicate varying extents of plagioclase and alkali feldspar fractionation.

The Rushan gabbro-diorite samples have overall low MgO and Ni but show positive correlation between MgO and Ni, suggesting fractional crystallization of olivine (Fig. 9a). Clinopyroxene fractionation is indicated by positive correlations between MgO and Cr or CaO (Fig. 9b, c), consistent with abundant clinopyroxene phenocrysts in the Rushan samples. Plagioclase fractionation is responsible for moderate negative Eu anomalies (Fig. 5a) according to positive correlation between Eu/Eu* and Sr/Sr* or Sr/Y in the Rushan samples (Fig. 9d, e).

5.1.2. Crustal contamination

Both the Rushan and Wulian samples exhibit significant depletion of Nb, Ta and Ti (Fig. 5b) and have strongly negative bulk-rock $\varepsilon_{Nd}(t)$ and
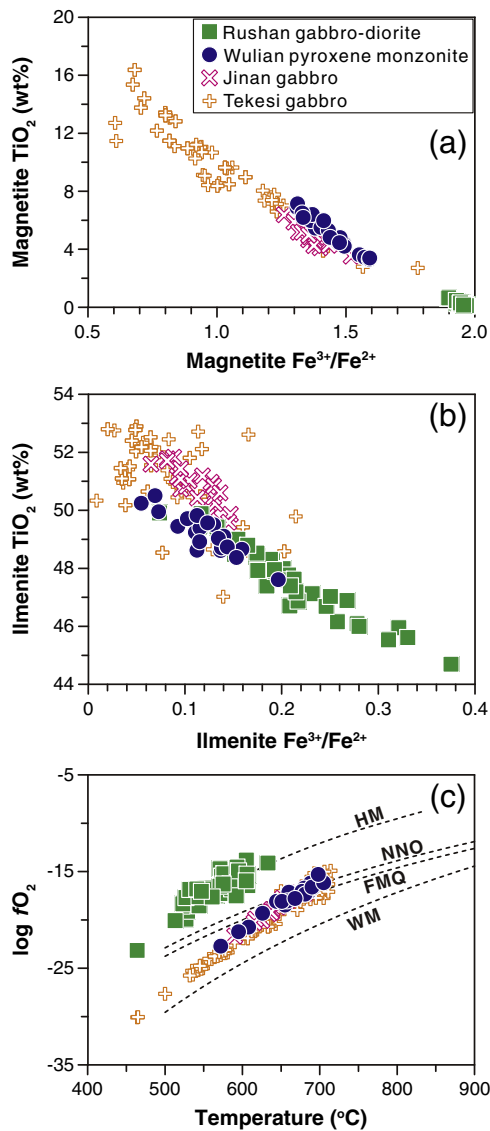
Fig. 8. Plots of (a) magnetite TiO_2 vs. Fe^{3+}/Fe^{2+}; (b) ilmenite TiO_2 vs. Fe^{3+}/Fe^{2+}; and (c) Oxygen-fugacity vs. temperature for Rushan gabbro-diorite and Wulian pyroxene monzonite. The data of Jinan gabbros in the western Shangdong and Tekesi gabbro in the Southwest Tianshan orogen are shown for comparison. Oxygen-fugacity and temperature were estimated using magnetite-ilmenite geothermobarometry program (ILMAT120; Lepage, 2003). MN trajectory for magnetite–nickel buffer, NNO for nickel–nickel-oxide, FMQ for quartz–fayalite–magnetite and WM for wüstite–magnetite (Eugster and Wones, 1962).

$\varepsilon_{Hf}(t)$ values, high initial bulk-rock $^{87}Sr/^{86}Sr$ ratios (Fig. 6) and negative zircon $\varepsilon_{Hf}(t)$ values (Fig. 3c). Crustal contamination might be a possibility for negative Ta-Nb-Ti anomalies and enriched Sr-Nd-Hf isotopes. Extensive crustal contamination would be required for the strong depletion of Nb, Ta and Ti and strongly negative $\varepsilon_{Nd}(t)$ values, high initial $^{87}Sr/^{86}Sr$ ratios in the Wulian and Rushan samples. However, for an extensive crustal contamination, Sr-Nd-Hf isotope compositions would be correlated with SiO_2, MgO and/or Nb/La, which are not observed in both suites (Fig. 10). This, in turn, precludes the possibility of extensive crustal contamination.

5.1.3. Mantle source metasomatized by Triassic continental subduction

Partial melting of an unmodified upper mantle peridotite cannot adequately produce the strongly negative Nb-Ta-Ti anomalies and pronounced enrichment of incompatible elements seen in Fig. 5b. Fractional crystallization of Ti-bearing minerals such as rutile or amphibole has notable effect on Ta-Nb-Ti depletion (Klemme et al., 2005; Tiepolo et al.,

2000). Relatively high and constant Dy/Yb ratios of the Rushan and Wulian samples ($[Dy/Yb]_N = 1.39–1.78$; Supplemental Table 3) would argue against the notable effect of amphibole crystallization. Both the Rushan and Wulian samples have chondritic or slightly subchondritic Nb/Ta ratios of 15.7–17.8 (Supplemental Table 3) (chondritic Nb/Ta ratio = 17.4; Sun and McDonough, 1989), distinctly contradicting with rutile crystallization that will result in superchondritic Nb/Ta ratios in the residual melts (Klemme et al., 2005).

Collectively, geochemical and isotopic characteristics of the Rushan and Wulian rocks are most likely derived from a mantle source that was enriched in Sr-Nd-Hf isotopes but depleted in Ta-Nb-Ti. The enrichment degree of LREE and LILE for the Rushan and Wulian rocks is higher than those for the coeval igneous rocks from the interior of the NCC, for example the Jinan and Zouping gabbros (Figs. 5, 6). This suggests that the mantle source for the Rushan and Wulian rocks have experienced more intensive metasomatism. Such a mantle source may have been formed by hybridization of the mantle source by recycled terrigenous sediments (Conticelli and Peccerillo, 1992; Hawkesworth et al., 1993) or by fluid released from supra-subduction zone (Donnelly et al., 2004; Tatsumi, 1986).

According to zircon SIMS U-Pb dating results, both the Wulian (123.0 ± 1.4 Ma) and Rushan (114.5 ± 0.5 Ma) rocks were formed immediately after or simultaneous with the northwestward drifting of Pacific plate at ~125 — 122 Ma (Sun et al., 2007). While a recent oceanic crust subduction accounts for the enrichment of large-ion-lithophile (LIL) elements and depletion of high-field-strength (HFS) elements, it cannot account for radiogenic Sr and unradiogenic Nd and Hf isotopic compositions observed in the Rushan and Wulian samples (Fig. 6).

Some samples from the Rushan intrusion and all samples from the Wulian intrusion exhibit variable degrees of decoupling between Hf and Nd isotopes (Fig. 6b). For a given ε_{Nd} value, oceanic crust has a lower while the global subducted sediment (GLOSS) has a higher ε_{Hf} value relative to the mantle array (Fig. 6b; Chauvel et al., 2008). The involvement of oceanic crust and/or subducted sediment can generate the decoupling between Hf and Nd isotopes in the mantle source (e.g., Chauvel et al., 2008; Li et al., 2014). If so, strongly negative ε_{Nd} and ε_{Hf} of the Rushan and Wulian rocks would require the involvement of ancient (>1.0 Ga) oceanic crust and/or subducted sediment (Fig. 6b). It is noteworthy that the Rushan and Wulian rocks have much more unradiogenic Hf–Nd isotopic compositions than the marine sediments from the northwestern Pacific (Vervoort et al., 2011) (Fig. 6b). This suggests that the decoupling between Hf and Nd isotopes cannot be due to the western Pacific subduction beneath East Asia in the Early Cretaceous, but is likely attributed to ancient crustal materials recycled into mantle source.

Widespread adakitic rocks in Jiaodong area, mainly formed during the Late Jurassic to Early Cretaceous (Fig. 11a, b), were mostly related to post-collisional processes of the Sulu orogen. The high-MgO adakitic rocks in the Early Cretaceous (Fig. 11c) were probably due to the lithospheric delamination (Liu et al., 2009), while other low-MgO adakitic rocks in the Late Jurassic to Early Cretaceous (Fig. 11) were likely derived from partial melting of thickened lower crust (Hou et al., 2007; Liu et al., 2009; Ma et al., 2013; Yang et al., 2003; Zhang et al., 2010b). Therefore, Mesozoic adakitic rocks in Jiaodong area, characterized by overall high initial $^{87}Sr/^{86}Sr$, remarkably negative bulk-rock $\varepsilon_{Nd}(t)$ and zircon $\varepsilon_{Hf}(t)$ values (Figs. 6a, 11d), would hold the geochemical features of the ancient crustal materials in the mantle source beneath the Sulu orogen. Both the Rushan and Wulian intrusions, located at the Sulu orogen, are tectonically and geochemically affiliated to the southern margin of the NCC. Consistently, bulk-rock Sr-Nd isotopes and zircon Hf isotopes of the Rushan and Wulian rocks were all similar to those of Late Jurassic to Early Cretaceous adakitic rocks in the Sulu orogen (Figs. 6a, 11d), which indicates that the metasomatism of mantle source was most likely associated with the processes responsible for the Sulu orogeny. Accordingly, the decoupling between Hf and Nd isotopes of the Rushan and Wulian rocks would be due to subduction/collision or
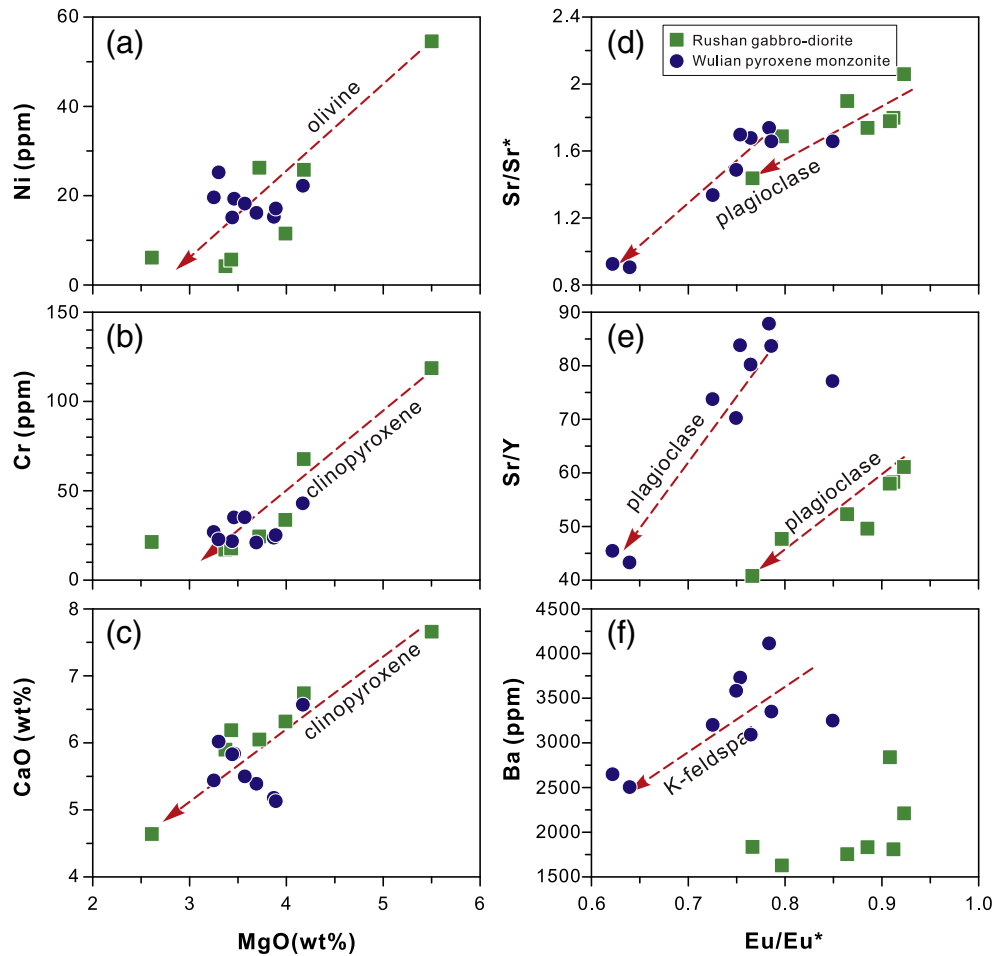
Fig. 9. Plots of (a) Ni vs. MgO; (b) Cr vs. MgO; (c) CaO vs. MgO; (d) Sr/Sr* vs. Eu/Eu*; (e) Sr/Y vs. Eu/Eu*; and (f) Ba vs. Eu/Eu* for Rushan gabbro-diorite and Wulian pyroxene monzonite. Sr/Sr* = 2 × Sr$_{PM}$/[Sm$_{PM}$ + Nd$_{PM}$]; PM normalization factors are from Sun and McDonough (1989).

post-orogenic collapse in the Sulu orogen. The Wulian samples show overall larger degree of decoupling between Hf and Nd isotopes than the Rushan samples (Fig. 6b), indicating a more extensive crustal materials recycled into mantle source, consistent with higher potassium of the rocks (Fig. 4f).

5.2. Hydration of the mantle source by Pacific subduction

The Paleo-Pacific subduction is regarded as one of principal triggers of the destruction of the NCC (Xu, 2014; Xu et al., 2004a, 2012; Zhu et al., 2012a, 2012b). The widespread NNE-trending basins in the eastern NCC, mainly formed during the Cretaceous–Paleogene (Ren et al., 2002), may have been induced by the Pacific subduction. Such a geodynamic process is supported by the findings of significant contribution of recycled oceanic crust (ROC) in the genesis of < 90 Ma basalts (Sakuyama et al., 2013; Xu, 2014; Xu et al., 2012; Yu et al., 2010; Zhang et al., 2009). Essentially, geochemical evidence of ROC was based on the studies on the OIB-type basalts derived from partial melting of asthenosphere source (Sakuyama et al., 2013; Xu, 2014; Xu et al., 2012; Zhang et al., 2009). Involvement of large amounts of lithosphere materials in the source during the dominant destruction of the NCC in the early Cretaceous would cause difficulties in evaluating the component of ROC. However, if the Mesozoic geodynamics was controlled by the Pacific subduction, the lithospheric mantle source underneath the eastern NCC may have been hydrated similar to the overlying mantle wedge above the subducting plate.

Fluorine and chlorine are ubiquitous volatile components in mantle- and crust-derived magmas and continental crystalline rocks (e.g., Aoki

et al., 1981; Bucher and Stober, 2010; Zhang et al., 2012) and thus represent the potential tracer for recycled oceanic crust and volatile-rich mantle source. Cl is most likely to escape in hydrous slab fluids during slab devolatilization, whereas F is largely returned to the deep mantle (e.g., Dixon et al., 2002; Ito et al., 1983; Schilling et al., 1978; Zhu and Sverjensky, 1991). Thus, Cl and H$_2$O would be efficiently fractionated from F during the subduction process (Straub and Layne, 2003). As a result, island arc basalts have lower F/Cl ratios than the subducted crust (Ito et al., 1983; Straub and Layne, 2003), while OIB source mantle is enriched in F through recycling of subducted oceanic crust (Kovalenko et al., 2006). Hydrous minerals such as amphibole and biotite can be used to decipher halogen concentrations in the melts, which might illuminate the source variations of Cl and F. The presence of abundant biotites in the Rushan and Wulian mafic intrusions implies a hydrous source. The biotites in the Rushan samples have lower F and F/Cl but overall higher Cl than those in the Wulian samples, which would be due to distinct mantle sources with respect to halogens or different extents of fractional crystallization of hydrous mineral apatite or amphibole. Both the Rushan and Wulian rocks show the REE patterns of progressive decrease in HREE with increasing atomic number (Fig. 5a), arguing against significant amphibole fractionation. At low melt Cl contents, Cl is slightly incompatible and F is compatible with respect to apatite (Mathez and Webster, 2005). Thus, apatite fractionation will deplete the residual melt in F concentration and F/Cl ratio. However, apatite as an accessory mineral is impractical for producing significant variation on halogens in the residual melt. On the other hand, both F concentrations and F/Cl ratios of the Wulian samples are much higher than those of the Rushan samples despite of overlaps of major elements
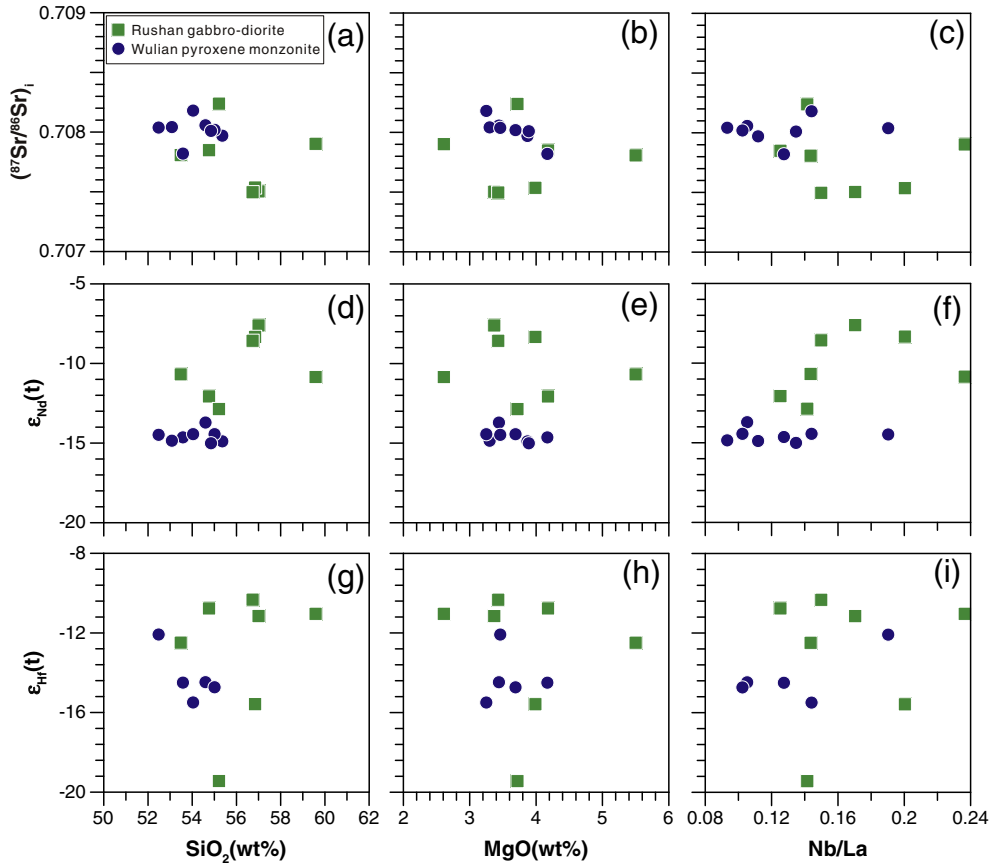
Fig. 10. Plots of Sr-Nd-Hf isotopes vs. SiO₂, MgO and Nb/La for Rushan gabbro-diorite and Wulian pyroxene monzonite.
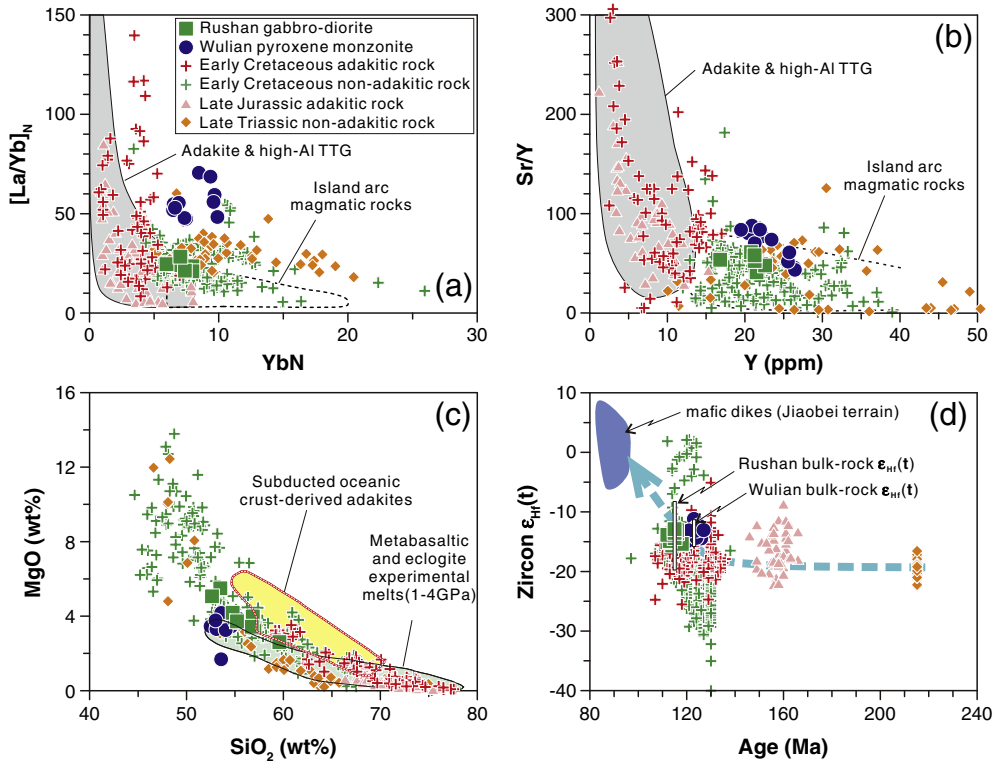

Fig. 11. Plots of (a) (La/Yb)$_N$ vs. Yb$_N$; (b) Sr/Y vs. Y; (c) MgO vs. SiO₂; and (d) zircon ε$_{Hf}$(t) vs. age for Rushan gabbro-diorite and Wulian pyroxene monzonite and other Mesozoic igneous rocks in the Jiaodong area. The Mesozoic igneous rocks in Jiaodong area shown for comparison are based on the literatures (Cai et al., 2013; Gao et al., 2004b; Goss et al., 2010; Guo et al., 2004; Hou et al., 2007; Hu et al., 2005, 2007; Lan et al., 2011; Li et al., 2012; Liu et al., 2008, 2009, 2011, 2012a; Ma et al., 2013, 2014a, 2014b; Meng et al., 2006; Tang et al., 2009, 2014; Wang et al., 2014; Yang and Wu, 2009; Yang et al., 2003, 2005a, 2005b; Zhang et al., 2006, 2010a, 2010b).

(Fig. 4), suggesting that the fractional crystallization of minerals including apatite cannot be major process for the contrastive F and Cl concentrations between Wulian and Rushan rocks. Thus, contrasting mantle sources with respect to halogens would be the essence of different biotites of the two areas. In other words, mantle source in the eastern Sulu orogen contains more aqueous fluid than that in western Sulu orogen, consistent with the geometry of Pacific subduction system (Fig. 12). Within this scheme, H_2O-rich fluid in the mantle beneath the Rushan area, closer to mantle wedge, was most likely released from subducted slab at shallow depth, while F-bearing fluid in the mantle beneath the Wulian area, far away from mantle wedge, was dominantly derived through recycling of subducted oceanic crust (Fig. 12). Consistently, mantle source for the Jinan gabbro in the western Shandong, typical of the predominant ancient cratonic mantle beneath the interior of the southeastern NCC (Huang et al., 2012a), would be characterized by relatively higher F and F/Cl but lower Cl in comparison with that for the Rushan gabbro-diorite according to their halogens in the biotites (Fig. 7).

Such a lateral variation in fluid composition in mantle source beneath the Sulu orogen is consistent with the distinct redox states of the two mafic intrusions (Fig. 8c). The oxygen fugacities of the Wulian pyroxene monzonite calculated based on magnetite-ilmenite equilibration are lower than the nickel-nickel oxide buffer, similar to those of the Jinan gabbro in the interior of the NCC and the Tekesi gabbro in the Southwest Tianshan orogen, NW China (Fig. 8c). The Jinan gabbros were derived from partial melting of dominant proto-lithospheric mantle and subordinate asthenosphere (Huang et al., 2012a), while the Tekesi gabbro would be genetically related to the Tarim mantle plume (He et al., 2013), which are all irrelevant to dehydration of subducted oceanic crust. However, the oxygen fugacities of the Rushan gabbro-diorite are close to the hematite-magnetite buffer (Fig. 8c). If the oxidation is related to the addition of H_2O from the subducted slab (Kelley and Cottrell, 2009), the observed lateral variation in oxygen fugacity for the studied rocks is most likely caused by fluid processes associated with the subduction of paleo-Pacific plate.

It has been proposed that the Pacific subduction beneath the NCC was initiated in the Middle Jurassic (Engebretson et al., 1985; Wu et al., 2007) and had changed from highly oblique to orthogonal in the Late Jurassic to Early Cretaceous (Engebretson et al., 1985; Isozaki, 1997; Ratschbacher et al., 2000). Since that the Rushan gabbro-diorite formed ~8 Ma later than the Wulian pyroxene monzonite (Fig. 4), their diverse mantle sources might reflect the enhanced influence of the Pacific subduction. In this scenario, the mantle source for the mafic rocks at ~ 128–130 Ma in the interior of the NCC (Huang et al., 2012a) would not be directly hydrated by subducted Pacific plate within a mantle wedge. Nevertheless, it does not exclude the effect of fluids released from the stagnant oceanic slab within the mantle transition zone, and the influence of Pacific subduction can be traced back in time at least to Early Cretaceous.

5.3. Mechanism for magmatism during the principal lithosphere destruction in the Sulu orogenic belt

The geochronology data show four episodes of Mesozoic magmatism in the Jiaodong Peninsula: Late Triassic, Late Jurassic, Early Cretaceous and Late Cretaceous (Fig. 1b).

Late Triassic rocks are characterized by extremely high K_2O contents (Fig. 11a) and have relatively low initial $^{87}Sr/^{86}Sr$ ratios, $\varepsilon_{Nd}(t)$ values and zircon $\varepsilon_{Hf}(t)$ values (Figs. 6a, 11b and 11c). The syenites have affinities with A-type granite, which are post-orogenic magmatism in an extensional setting of the Sulu orogenic belt (Yang et al., 2005a) after the continental collision.

Late Jurassic magmatism, dominantly recorded by the Linglong and Kunyushan granites (Fig. 1b) (Hou et al., 2007; Ma et al., 2013; Zhang et al., 2010b), have affinities with adakite in high Sr/Y and $[La/Yb]_N$ ratios and low Y and Yb contents (Fig. 11). They are characterized by low MgO, high SiO_2 and negative bulk-rock $\varepsilon_{Nd}(t)$ values and zircon $\varepsilon_{Hf}(t)$ values (Fig. 11), likely derived from partial melting of a thickened lower crust in the Sulu orogenic belt.

Early Cretaceous magmatism, extensively in the Jiaodong Peninsula, exhibits wide composition with variable bulk-rock $\varepsilon_{Nd}(t)$ values and zircon $\varepsilon_{Hf}(t)$ values (Fig. 11) (Hu et al., 2005, 2007; Huang et al., 2006; Lan et al., 2011; Liu et al., 2008, 2009; Meng et al., 2005, 2006; Tang et al., 2009; Yang et al., 2005b). Most Early Cretaceous rocks, including the Rushan gabbro-diorite and Wulian pyroxene monzonite, have relatively
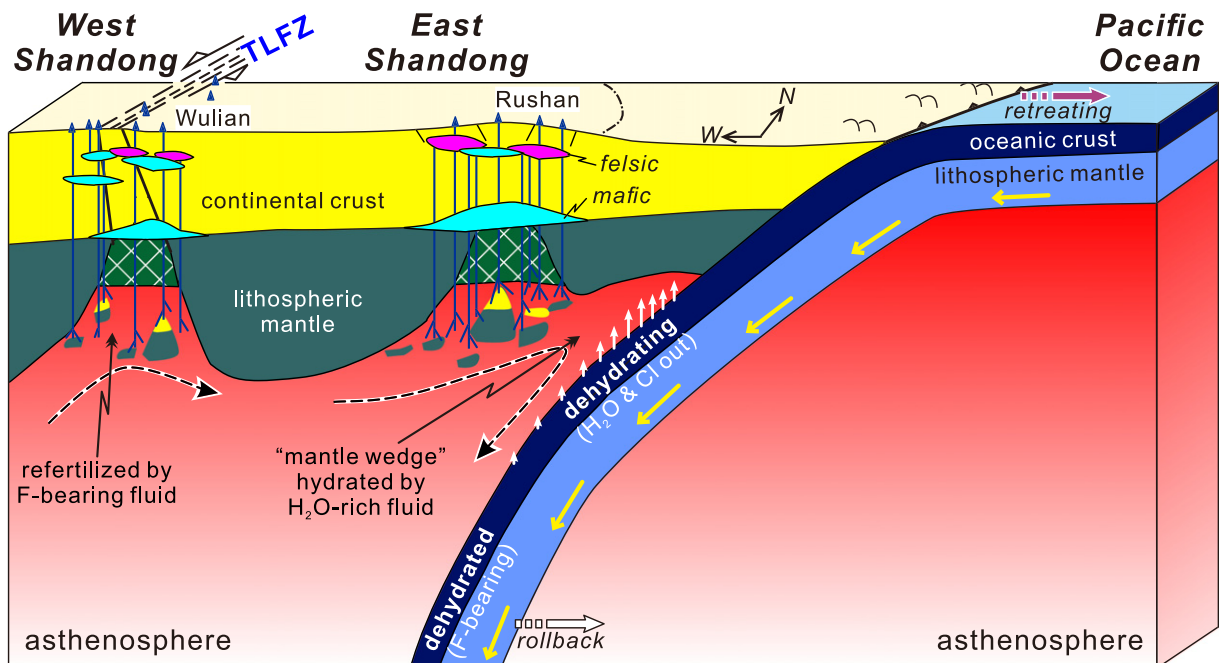

Fig. 12. Cartoon showing the roles of the Pacific oceanic subduction on lithospheric thinning beneath the Sulu orogenic belt and Tan-Lu fault zone in the early Cretaceous.

high K$_2$O and show wide ranges of SiO$_2$ and MgO, belong to Shoshonite series or high-potassium calc-alkaline series (Fig. 11a). The high-Ti lamprophyre dikes in the Jiaojia gold deposit might originate from partial melting of a convective asthenospheric mantle (Ma et al., 2014a). In addition, a small amount of Early Cretaceous rocks, such as some volcanic rocks in the Wulian area (Liu et al., 2009) and granitic rocks at Sanfoshan (Zhang et al., 2006, 2010b) and Guojialing (Hou et al., 2007; Yang et al., 2003), have overall high SiO$_2$ but relatively low K$_2$O, and show affinities with adakite (Fig. 11). Some Early Cretaceous adakitic rocks have low MgO and high SiO$_2$ similar to the Late Jurassic adakites, which would be derived from partial melting of a thickened lower crust (Zhang et al., 2010b), while some with high-MgO contents (Fig. 11) would be related to the lithospheric delamination (Liu et al., 2009).

Late Cretaceous magmatism is recorded by mafic dikes in the Jiaobei terrain. The dikes show variable initial ^{87}Sr/^{86}Sr values with positive bulk-rock ε_{Nd}(t) values and zircon ε_{Hf}(t) values (Fig. 11), which was interpreted to be from a newly accreted depleted lithospheric mantle source (Cai et al., 2013).

Collectively, four episodes of Mesozoic magmatic rocks in the Jiaodong Peninsula record a tectonic transformation of the Sulu Orogen, as the sequence of lithospheric evolution. The notable transformation of mantle source from enriched lithosphere in the Early Cretaceous to depleted mantle source in the Late Cretaceous indicates that the destruction of the lithosphere beneath the Sulu orogenic belt and periphery region took place principally during the Early Cretaceous. The Early Cretaceous mafic and intermediate rocks are all ultrapotassic or potassic (Fig. 11a), likely derived from partial melting of predominant enriched lithosphere mantle and minor upwelling asthenosphere. Furthermore, high initial ^{87}Sr/^{86}Sr, low negative bulk-rock ε_{Nd}(t) and ε_{Hf}(t) values and zircon ε_{Hf}(t) values of the Rushan and Wulian rocks (Figs. 6 and 11) require significant old crustal materials recycled into mantle source, probably through the collision between SCB and NCC and subsequent orogenic collapse in the Late Triassic. The lower crustal delamination, if occurring in the early Cretaceous, would also be partially responsible for enrichment of mantle source. A holistic delamination of subcontinental lithosphere is not a viable mechanism to induce the destruction of the lithosphere within the North China Craton, but it is possible that the delamination occurred on the marginal orogens (Gu et al., 2013; Huang et al., 2012a; Li and Huang 2013; Windley et al., 2010). Therefore, continental collision between the SCB and NCC and consequent post-collisional processes in the Dabie and Sulu orogens and periphery region had exerted important influence on lithospheric thinning in the southeastern NCC (e.g., Huang et al., 2012a; Liu et al., 2012b; Xu et al., 2009; Yang et al., 2012a, 2012b; Zhang and Gao, 2002; Zhang et al., 2002).

However, it is enigmatic that the most extensive magmatism (Early Cretaceous; Fig. 1b) coeval with the dominant lithospheric thinning is more than 100 Ma after the continental collision between the SCB and NCC. It is interesting to note that there is a spatially heterogeneous mantle source with respect to halogens contents and oxygen fugacity beneath the Sulu orogenic belt in the Early Cretaceous (Fig. 12). The lateral variation is consistent with the geometry of Pacific subduction system, indicating that the juxtaposition of Pacific subduction would be the most likely mechanism for the extensive magmatism in the Early Cretaceous. Such a geodynamic process would not only trigger the partial melting of mantle wedge, but also induce asthenosphere convection in the interior of the NCC due to wedge-suction (Niu, 2005; Niu et al., 2015) (Fig. 12). The weakened lithospheric zones such as the Dabie-Sulu orogens and Tan-Lu fault zone along the cratonic margins would became the favorable site for extensive magmatism (Gu et al., 2013; Huang et al., 2012a; Xu et al., 2009) with melting of hybrid mantle sources such as metasomatism lithospheric mantle and ascending asthenosphere. Therefore, magmatic rocks in the early Cretaceous have much wide ranges of Nd-Hf isotopes than other episodes of magmatic rocks (Fig. 11).

6. Conclusions

The Rushan gabbro-diorite and Wulian pyroxene monzonite in the Early Cretaceous (115 ± 1 Ma and 123 ± 1 Ma, respectively) represent typical mafic magmatism in the Sulu orogen during the dominant destruction of the NCC. They are characterized by high potassium, high initial ^{87}Sr/^{86}Sr, strongly negative ε_{Nd}(t) and ε_{Hf}(t), as well as notable negative Ta, Nb and Ti anomalies, predominantly attributed to partial melting of enriched lithosphere mantle refertilized by recycled crustal materials responsible for the Sulu orogeny.

Consistent with the geometry of Pacific subduction system, there is a spatially heterogeneous Cretaceous mantle source with respect to halogens and water contents beneath the Sulu orogen. The Pacific subduction played an important role in the dominant destruction of the NCC since the Early Cretaceous.

Supplementary data to this article can be found online at http://dx.doi.org/10.1016/j.lithos.2016.02.008.

References

Aoki, K., Ishiwaka, K., Kanisawa, S., 1981. Fluorine geochemistry of basaltic rocks from continental and oceanic regions and petrogenetic application. Contributions to Mineralogy and Petrology 76, 53–59.
Bucher, K., Stober, I., 2010. Fluids in the upper continental crust. Geofluids 10, 241–253.
Cai, Y.C., Fan, H.R., Santosh, M., Liu, X., Hu, F.F., Yang, K.F., Lan, T.G., Yang, Y.H., Liu, Y.S., 2013. Evolution of the lithospheric mantle beneath the southeastern North China Craton: Constraints from mafic dikes in the Jiaobei terrain. Gondwana Research 24, 601–621.
Chauvel, C., Lewin, E., Carpentier, M., Arndt, N.T., Marini, J.C., 2008. Role of recycled oceanic basalt and sediment in generating the Hf–Nd mantle array. Nature Geoscience 1, 64–67.
Chen, J.F., Xie, Z., Li, H.M., Zhang, X.D., Zhou, T.X., Park, Y.S., Ahn, K.S., Chen, D.G., Zhang, X., 2003. U–Pb zircon ages for a collision-related K-rich complex at Shidao in the Sulu ultrahigh pressure terrane, China. Geochemical Journal 37, 33–46.
Chu, N.C., Taylor, R.N., Chavagnac, V., Nesbitt, R.W., Boella, R.M., Milton, J.A., German, C.R., Bayon, G., Burton, K., 2002. Hf isotope ratio analysis using multi-collector inductively coupled plasma mass spectrometry: an evaluation of isobaric interference corrections. Journal of Analytical Atomic Spectrometry 17, 1567–1574.
Conticelli, S., Peccerillo, A., 1992. Petrology and geochemistry of potassic and ultrapotassic volcanism in Central Italy – petrogenesis and inferences on the evolution of the mantle sources. Lithos 28, 221–240.
Deng, J.F., Su, S.G., Niu, Y.L., Liu, C., Zhao, G.C., Zhao, X.G., Zhou, S., Wu, Z.X., 2007. A possible model for the lithospheric thinning of North China Craton: Evidence from the Yanshanian (Jura-Cretaceous) magmatism and tectonism. Lithos 96, 22–35.
Dixon, J.E., Leist, L., Langmuir, C.H., Schilling, J.G., 2002. Recycled dehydrated lithosphere observed on plume-influenced mid-ocean ridge basalts. Nature 420, 385–389.
Donnelly, K.E., Goldstein, S.L., Langmuir, C.H., Spiegelman, M., 2004. Origin of enriched ocean ridge basalts and implications for mantle dynamics. Earth and Planetary Science Letters 226, 347–366.
Engebretson, D.C., Cox, A., Gordon, R.G., 1985. Relative motion between oceanic and continental plates in the Pacific basin. Geological Society of America Special Papers 206, 1–55.
Eugster, H.P., Wones, D.R., 1962. Stability relations of the ferruginous biotite, annite. Journal of Petrology 3, 82–125.
Fan, W.M., Zhang, H.F., Baker, J., Javis, K.E., Mason, P.R.D., Menzies, M.A., 2000. On and off the North China craton: where is the Archean keel? Journal of Petrology 41, 933–950.
Fan, W.M., Guo, F., Wang, Y.J., Lin, G., Zhang, M., 2001. Post-orogenic bimodal volcanism along the Sulu orogenic belt in Eastern China. Physics and Chemistry of the Earth (A) 26, 733–746.
Fukao, Y., Obayashi, M., Inoue, H., Nenbai, M., 1992. Subducting slab stagnant in the mantle transition zone. Journal of Geophysical Research - Solid Earth 97, 4809–4822.
Gao, S., Rudnick, R.L., Carlson, R.W., McDonough, W.F., Liu, Y.S., 2002. Re–Os evidence for replacement of ancient mantle lithosphere beneath the North China Craton. Earth and Planetary Science Letters 198, 307–322.
Gao, S., Rudnick, R.L., Yuan, H.L., Liu, X.M., Liu, Y.S., Xu, W.L., Ling, W.L., Ayers, J., Wang, X.C., Wang, Q.H., 2004a. Recycling lower continental crust in the North China craton. Nature 432, 892–897.

Gao, T.S., Chen, J.F., Xie, Z., Yan, J., Qian, H., 2004b. Geochemistry of Triassic igneous complex at Shidao in the Sulu UHP metamorphic belt. Acta Petrologica Sinica 20, 1025–1038 (in Chinese with English abstract).

Goss, S.C., Wilde, S.A., Wu, F.Y., Yang, J.H., 2010. The age, isotopic signature and significance of the youngest Mesozoic granitoids in the Jiaodong Terrance, Shandong Province, North China Craton. Lithos 120, 309–326.

Griffin, W.L., Zhang, A., O'Reilly, S.Y., Ryan, C.G., 1998. Phanerozoic evolution of the lithosphere beneath the Sino-Korean Craton. In: Flower, M.F.J., Chung, S.L., Lo, C.H., Lee, T.Y. (Eds.), Mantle dynamics and plate interaction in East Asia Geodynamics Series 27, pp. 107–126.

Griffin, W.L., Pearson, N.J., Belousova, E., Jackson, S.E., O'Reilly, S.Y., van Achterberg, E., Shee, S.R., 2000. The Hf isotope composition of cratonic mantle: LAM-MC-ICPMS analysis of zircon megacrysts in kimberlites. Geochimica et Cosmochimica Acta 64, 133–147.

Griffin, W.L., Pearson, N.J., Belousova, E.A., Saeed, A., 2006. Comment: Hf-isotope heterogeneity in zircon 91500. Chemical Geology 233, 358–363.

Gu, H.O., Xiao, Y., Santosh, M., Li, W.Y., Yang, X., Pack, A., Hou, Z., 2013. Spatial and temporal distribution of Mesozoic adakitic rocks along the Tan-Lu fault, Eastern China: Constraints on the initiation of lithospheric thinning. Lithos 177, 352–365.

Guo, F., Fan, W.M., Wang, Y.J., Zhang, M., 2004. Origin of early Cretaceous calc-alkaline lamprophyres from the Sulu orogen in eastern China: implications for enrichment processes beneath continental collisional belt. Lithos 78, 291–305.

Guo, J.H., Chen, F.K., Zhang, X.M., Siebel, W., Zhai, M.G., 2005. Evolution of syn- to post-collisional magmatism from north Sulu UHP belt, eastern China: zircon U–Pb geochronology. Acta Petrologica Sinica 21, 1281–1301 (in Chinese with English abstract).

Guo, F., Fan, W.M., Li, C.W., 2006. Geochemistry of late Mesozoic adakites from the Sulu belt, eastern China: magma genesis and implications for crustal recycling beneath continental collisional orogens. Geological Magazine 143, 1–13.

Hawkesworth, C.J., Gallagher, K., Hergt, J.M., McDermott, F., 1993. Mantle and slab contributions in arc magmas. Annual Review of Earth and Planetary Sciences 21, 175–204.

He, P.L., Huang, X.L., Li, H.Y., Li, J., Yu, Y., Li, W.X., 2013. Mechanism of Fe-Ti enrichment in the Haladala gabbros: Implication for the tectonic evolution of the western Tianshan orogenic belt. Acta Petrologica Sinica 29, 3457–3472 (in Chinese English abstract).

Hou, M.L., Jiang, Y.H., Jiang, S.Y., Ling, H.F., Zhao, K.D., 2007. Contrasting origins of late Mesozoic adakitic granitoids from the northwestern Jiaodong Peninsula, east China: implications for crustal thickening to delamination. Geological Magazine 144, 619–633.

Hu, F.F., Fan, H.R., Yang, J.H., Zhai, M.G., Jin, C.W., Xie, L.W., Yang, Y.H., 2005. Magma mixing for the origin of granodiorite: geochemical, Sr-Nd isotopic and zircon Hf isotopic evidence of dioritic enclaves and host rocks from Changshannan granodiorite in the Jiaodong Peninsula, eastern China. Acta Petrologica Sinica 21, 569–586 (in Chinese with English abstract).

Hu, F.F., Fan, H.R., Yang, J.H., Zhai, M.G., Xie, L.W., Yang, Y.H., Liu, X.M., 2007. Petrogenesis of Gongjia gabbro-diorite in the Kunyushan area, Jiaodong Peninsula: constraints from petro-geochemistry, zircon U-Pb dating and Hf isotopes. Acta Petrologica Sinica 23, 369–380 (in Chinese with English abstract).

Huang, J., Zheng, Y.F., Zhao, Z.F., Wu, Y.B., Zhou, H.B., Liu, X.M., 2006. Melting of subducted continent: element and isotopic evidence for a genetic relationship between Neoproterozoic and Mesozoic granitoids in the Sulu orogen. Chemical Geology 229, 227–256.

Huang, X.L., Niu, Y.L., Xu, Y.G., Yang, Q.J., Zhong, J.W., 2010. Geochemistry of TTG and TTG-like gneisses from Lushan-Taihua Complex in the southern North China Craton: implications for late Archean crustal accretion. Precambrian Research 182, 43–56.

Huang, X.L., Zhong, J.W., Xu, Y.G., 2012a. Two tales of the continental lithospheric mantle prior to the destruction of the North China Craton: insights from Early Cretaceous mafic intrusions in western Shandong, East China. Geochimica et Cosmochimica Acta 96, 193–214.

Huang, X.L., Wilde, S.A., Yang, Q.J., Zhong, J.W., 2012b. Geochronology and Petrogenesis of grey gneisses from the Taihua Complex at Xiong'er in the southern segment of the Trans-North China Orogen: implications for tectonic transformation in the Early Paleoproterozoic. Lithos 134, 236–252.

Huang, X.L., Wilde, S.A., Zhong, J.W., 2013. Episodic crustal growth in the southern segment of the Trans-North China Orogen across the Archean-Proterozoic boundary. Precambrian Research 233, 337–357.

Iizuka, T., Hirata, T., 2005. Improvements of precision and accuracy in in-situ Hf isotope microanalysis of zircon using the laser ablation-MC-ICPMS technique. Chemical Geology 220, 121–137.

Isozaki, Y., 1997. Jurassic accretion tectonics of Japan. Island Arc 6, 25–51.

Ito, E., Harris, D., Anderson, A.T., 1983. Alteration of oceanic crust and geologic cycling of chlorine and water. Geochimica et Cosmochimica Acta 47, 1613–1624.

Kelley, K.A., Cottrell, E., 2009. Water and the Oxidation state of subduction zone magmas. Science 325, 605–607.

Klemme, S., Prowatke, S., Hametner, K., Gunther, D., 2005. Partitioning of trace elements between rutile and silicate melts: implications for subduction zones. Geochimica et Cosmochimica Acta 69, 2361–2371.

Kovalenko, V., Naumov, V., Girnis, A., Dorofeeva, V., Yarmolyuk, V., 2006. Composition and chemical structure of oceanic mantle plumes. Petrology 14, 452–476.

Lan, T.G., Fan, H.R., Hu, F.F., Tomkins, A.G., Yang, K.F., Liu, Y.S., 2011. Multiple crust– mantle interactions for the destruction of the North China Craton: geochemical and Sr–Nd–Pb–Hf isotopic evidence from the Longbaoshan alkaline complex. Lithos 122, 87–106.

Lepage, L.D., 2003. ILMAT: an Excel worksheet for ilmenite-magnetite geothermometry and geobarometry. Computers & Geosciences 29, 673–678.

Li, H.Y., Huang, X.L., 2013. Constraints on the paleogeographic evolution of the North China Craton during the Late Triassic–Jurassic. Journal of Asian Earth Sciences 70– 71, 308–320.

Li, S.G., Huang, F., Li, H., 2002. Post-collisional lithosphere delamination of the Dabie-Sulu orogen. Chinese Science Bulletin 47, 259–263.

Li, X.H., Li, Z.X., Wingate, M.T.D., Chung, S.L., Liu, Y., Lin, G.C., Li, W.X., 2006. Geochemistry of the 755 Ma Mundine Well dyke swarm, northwestern Australia: part of a Neoproterozoic mantle superplume beneath Rodinia? Precambrian Research 146, 1–15.

Li, X.H., Liu, Y., Li, Q.L., Guo, C.H., Chamberlain, K.R., 2009. Precise determination of Phanerozoic zircon Pb/Pb age by multicollector SIMS without external standardization. Geochemistry, Geophysics, Geosystems 10, Q04010. http://dx.doi.org/10.1029/2009GC002400.

Li, X.C., Fan, H.R., Santosh, M., Hu, F.F., Yang, K.F., Lan, T.G., Liu, Y.S., Yang, Y.H., 2012. An evolving magma chamber within extending lithosphere: An integrated geochemical, isotopic and zircon U–Pb geochronological study of the Gushan granite, eastern North China Craton. Journal of Asian Earth Sciences 50, 27–43.

Li, H.Y., Huang, X.L., Guo, H., 2014. Geochemistry of Cenozoic basalts from the Bohai Bay Basin: Implications for a heterogeneous mantle source and lithospheric evolution beneath the eastern North China Craton. Lithos 196, 54–66.

Liu, S., Hu, R.Z., Gao, S., Feng, C.X., Qi, Y.Q., Wang, T., Feng, G.Y., Coulson, I.M., 2008. U–Pb zircon age, geochemical and Sr–Nd–Pb–Hf isotopic constraints on age and origin of alkaline intrusions and associated mafic dikes from Sulu orogenic belt, east China. Lithos 106, 365–379.

Liu, S., Hu, R.Z., Gao, S., Feng, C.X., Yu, B.B., Qi, Y.Q., Wang, T., Feng, G.Y., Coulson, I.M., 2009. Zircon U-Pb age, geochemistry and Sr-Nd-Pb isotopic compositions of adakitic volcanic rocks from Jiaodong, Shandong Province, Eastern China: Constraints on petrogenesis and implications. Journal of Asian Earth Sciences 35, 445–458.

Liu, S., Hu, R.Z., Gao, S., Feng, C.X., Zhang, H., Qi, Y.Q., Wang, T., Feng, G.Y., Yang, Y.H., 2011. U–Pb zircon ages, geochemical and Sr–Nd–Pb isotopic constraints on the dating and origin of intrusive complexes in the Sulu orogen, eastern China. International Geology Review 53, 61–83.

Liu, S., Hu, R.Z., Gao, S., Feng, C.X., Feng, G.Y., Qi, Y.Q., Coulson, I.M., Yang, Y.H., Yang, C.G., Tang, L., 2012a. Geochemical and isotopic constraints on the age and origin of mafic dikes from eastern Shandong Province, eastern North China Craton. International Geology Review 54, 1389–1400.

Liu, S.A., Li, S.G., Guo, S.S., Hou, Z.H., He, Y.S., 2012b. The Cretaceous adakitic-basaltic-granitic magma sequence on south-eastern margin of the North China Craton: implications for lithospheric thinning mechanism. Lithos 134–135, 163–178.

Ludwig, K.R., 2003. Isoplot: a geochronological toolkit for Microsoft Excel. Berkeley Geochronology Centre Special Publication No. 4.

Ma, L., Jiang, S.Y., Dai, B.Z., Jiang, Y.H., Hou, M.L., Pu, W., Xu, B., 2013. Multiple sources for the origin of Late Jurassic Linglong adakitic granite in the Shandong Peninsula, eastern China: Zircon U–Pb geochronological, geochemical and Sr–Nd–Hf isotopic evidence. Lithos 162, 251–263.

Ma, L., Jiang, S.Y., Hofmann, A.W., Dai, B.Z., Hou, M.L., Zhao, K.D., Chen, L.H., Li, J.W., Jiang, Y.H., 2014a. Lithospheric and asthenospheric sources of lamprophyres in the Jiaodong Peninsula: A consequence of rapid lithospheric thinning beneath the North China Craton? Geochimica et Cosmochimica Acta 124, 250–271.

Ma, L., Jiang, S.Y., Hou, M.L., Dai, B.Z., Jiang, Y.H., Yang, T., Zhao, K.D., Pu, W., Zhu, Z.Y., Xu, B., 2014b. Geochemistry of Early Cretaceous calc-alkaline lamprophyres in the Jiaodong Peninsula: Implication for lithospheric evolution of the eastern North China Craton. Gondwana Research 25, 859–872.

Mathez, E.A., Webster, J.D., 2005. Partitioning behavior of chlorine and fluorine in the system apatite-silicate melt-fluid. Geochimica et Cosmochimica Acta 69, 1275–1286.

McArthur, J.M., 1994. Recent trends in strontium isotope stratigraphy. Terra Nova 6, 331–358.

Meng, F.C., Xue, H.M., Li, T.F., Yang, H.R., Liu, F.L., 2005. Enriched characteristics of late Mesozoic mantle under the Sulu orogenic belt: geochemical evidence from gabbro in Rushan. Acta Petrologica Sinica 21, 1583–1592 (in Chinese with English abstract).

Meng, F.C., Shi, R.D., Li, T.F., Liu, F.L., Xu, Z.Q., 2006. The ages and sources of Late Mesozoic granites in Southern Sulu Region. Acta Geologica Sinica 80, 1867–1876 (in Chinese with English abstract).

Menzies, M.A., Xu, Y.G., 1998. Geodynamics of the North China Craton. In: Flower, M.F.J., Chung, S.L., Lo, C.H., Lee, T.Y. (Eds.), Mantle dynamics and plate interactions in east Asia. AGU, Geodynamics Series 27, pp. 155–165.

Menzies, M.A., Fan, W.M., Zhang, M., 1993. Palaeozoic and Cenozoic lithoprobes and the loss of > 120 km of Archaean lithosphere, Sino-Korean craton, China. In: Prichard, H.M., Alabaster, T., Harris, N.B.W., Neary, C.R. (Eds.), Magmatic processes and plate tectonics. Geological Society Special Publication 76, pp. 71–78.

Miao, L.C., Luo, Z.K., Huang, J.Z., Guan, K., Wang, L.G., McNaughton, N.J., Groves, D.I., 1997. SHRIMP study of granitoid intrusions in Zhaoye Gold belt of Shandong province and its implications. Science in China (Series D) 40, 361–369 (in Chinese).

Niu, Y.L., 2005. Generation and evolution of basaltic magmas: some basic concepts and a new view on the origin of Mesozoic-Cenozoic basaltic volcanism in Eastern China. Geological Journal of China Universities 11, 9–46.

Niu, Y.L., Liu, Y., Xue, Q.Q., Shao, F.L., Chen, S., Duan, M., Guo, P.Y., Gong, H.M., Hu, Y., Hu, Z.X., Kong, J.J., Li, J.Y., Liu, J.J., Sun, P., Sun, W.L., Ye, L., Xiao, Y.Y., Zhang, Y., 2015. Exotic origin of the Chinese continental shelf: new insights into the tectonic evolution of the western Pacific and eastern China since the Mesozoic. Scientific Bulletin 60, 1598–1616.

Plank, T., Langmuir, C.H., 1998. The chemical composition of subducting sediment and its consequences for the crust and mantle. Chemical Geology 145, 325–394.

Qiu, J.S., Wang, D.Z., Luo, Q.H., Liu, H., 2001. ^{40}Ar-^{39}Ar dating for volcanic rocks of Qingshan Formation in Jiaolai basin, Eastern Shandong province: A case study of the Fenlingshan volcanic apparatus in Wulian County. Geological Journal of China Universities 7, 351–355 (in Chinese with English abstract).

Ratschbacher, L., Hacker, B.R., Webb, L.E., McWilliams, M., Ireland, T., Dong, S., Calvert, A., Chateigner, D., Wenk, H.R., 2000. Exhumation of the ultrahigh-pressure continental crust in east central China: Cretaceous and Cenozoic unroofing and the Tan-Lu fault. Journal of Geophysical Research 105, 13303–13338.

Ren, J., Tamaki, K., Li, S., Zhang, J., 2002. Late Mesozoic and Cenozoic rifting and its dynamic setting in eastern China and adjacent areas. Tectonophysics 344, 175–205.

Sakuyama, T., Tian, W., Kimura, J.I., Fukao, Y., Hirahara, Y., Takahashi, T., Senda, R., Chang, Q., Miyazaki, T., Obayashi, M., 2013. Melting of dehydrated oceanic crust from the stagnant slab and of the hydrated mantle transition zone: constraints from Cenozoic alkaline basalts in eastern China. Chemical Geology 359, 32–48.

Schilling, J.G., Unni, C.K., Bender, M.L., 1978. Origin of chlorine and bromine in the oceans. Nature 273, 631–636.

Straub, S.M., Layne, G.D., 2003. The systematics of chlorine, fluorine, and water in Izu arc front volcanic rocks: implications for volatile recycling in subduction zones. Geochimica et Cosmochimica Acta 67, 4179–4203.

Sun, S.-s., McDonough, W.F., 1989. Chemical and isotopic systematics of oceanic basalts: implications for mantle composition and processes. In: Saunders, A.D., Norry, M.J. (Eds.), Magmatism in the Ocean Basins. Geological Society, London, Special Publication 42, pp. 313–345.

Sun, W.D., Ding, X., Hu, Y.H., Li, X.H., 2007. The golden transformation of the Cretaceous plate subduction in the west Pacific. Earth and Planetary Science Letters 262, 533–542.

Tang, H.Y., Zheng, J.P., Yu, C.M., 2009. Age and composition of the Rushan intrusive complex in the northern Sulu orogen, eastern China: petrogenesis and lithospheric mantle evolution. Geological Magazine 146, 199–215.

Tang, H.Y., Zheng, J.P., Yu, C.M., Ping, X.Q., Ren, H.W., 2014. Multistage crust–mantle interactions during the destruction of the North China Craton: Age and composition of the Early Cretaceous intrusions in the Jiaodong Peninsula. Lithos 190, 52–70.

Tannaka, T., Togashi, S., Kamioka, H., Amakawa, H., Kagami, H., Hamamoto, T., Yuhara, M., Orihashi, Y., Yoneda, S., Shimizu, H., Kunimaru, T., Takahashi, K., Yanagi, T., Nakano, T., Fujimaki, H., Shinjo, R., Asahara, Y., Tnimizu, M., Dragusanu, C., 2000. JNdi-1: a neodymium isotopic reference in consistency with LaJolla neodymium. Chemical Geology 168, 279–281.

Tatsumi, Y., 1986. Formation of the volcanic front in subduction zones. Geophysical Research Letters 13, 717–720.

Taylor, S.R., McLennan, S.M., 1985. The Continental Crust: Its Composition and Evolution. Blackwell, Oxford.

Tiepolo, M., Vannucci, R., Oberti, R., Foley, S., Bottazzi, P., Zanetti, A., 2000. Nb and Ta incorporation and fractionation in titanian pargasite and kaersutite: crystal chemical constraints and implications for natural systems. Earth and Planetary Science Letters 176, 185–201.

Vervoort, J.D., Plank, T., Prytulak, J., 2011. The Hf-Nd isotopic composition of marine sediments. Geochimica et Cosmochimica Acta 75, 5903–5926.

Wang, Q., Wyman, A., Xu, J.F., Jian, P., Zhao, Z.H., Li, C.F., Xu, W., Ma, J.L., He, B., 2007. Early Cretaceous adakitic granites in the Northern Dabie complex, central China: implications for partial melting and delamination of thickened lower crust. Geochimica et Cosmochimica Acta 71, 2609–2636.

Wang, Z.L., Yang, L.Q., Deng, J., Santosh, M., Zhang, H.F., Liu, Y., Li, R.H., Huang, T., Zheng, X.L., Zhao, H., 2014. Gold-hosting high Ba-Sr granitoids in the Xincheng gold deposit, Jiaodong Peninsula, East China: Petrogenesis and tectonic setting. Journal of Asian Earth Sciences 95, 274–299.

Wiedenbeck, M., Alle, P., Corfu, F., Griffin, W.L., Meier, M., Oberli, F., Vonquadt, A., Roddick, J.C., Speigel, W., 1995. Three natural zircon standards for U-Th-Pb, Lu-Hf, trace-element and REE analyses. Geostandards Newsletter 19, 1–23.

Windley, B.F., Maruyama, S., Xiao, W.J., 2010. Delamination/thinning of sub-continental lithospheric mantle under eastern China: the role of water and multiple subduction. American Journal of Science 310, 1250–1293.

Wu, F.Y., Lin, J.Q., Wilde, S.A., Zhang, X.O., Yang, J.H., 2005. Nature and significance of the Early Cretaceous giant igneous event in Eastern China. Earth and Planetary Science Letters 233, 103–119.

Wu, F.Y., Yang, Y.H., Xie, L.W., Yang, J.H., Xu, P., 2006. Hf isotopic compositions of the standard zircons and baddeleyites used in U–Pb geochronology. Chemical Geology 234, 105–126.

Wu, F.Y., Yang, J.H., Lo, C.H., Wilde, S.A., Sun, D.Y., Jahn, B.M., 2007. The Heilongjiang Group: a Jurassic accretionary complex in the Jiamusi Massif at the western Pacific margin of northeastern China. Island Arc 16, 156–172.

Xie, L.W., Zhang, Y.B., Zhang, H.H., Sun, J.F., Wu, F.Y., 2008. In situ simultaneous determination of trace elements, U-Pb and Lu-Hf isotopes in zircon and baddeleyite. Chinese Science Bulletin 53, 1565–1573.

Xu, Y.G., 2001. Thermo-tectonic destruction of the Archean lithospheric keel beneath the Sino-Korean Craton in China: Evidence, Timing and Mechanism. Physics and Chemistry of the Earth (A) 26, 747–757.

Xu, Y.G., 2007. Diachronous lithospheric thinning of the North China Craton and formation of the Daxin'anling-Taihangshan gravity lineament. Lithos 96, 281–298.

Xu, Y.G., 2014. Recycled oceanic crust in the source of 90–40 Ma basalts in North and Northeast China: Evidence, provenance. Geochimica et Cosmochimica Acta 143, 49–67.

Xu, Y.G., Huang, X.L., Ma, J.L., Wang, Y.B., Iizuka, Y., Xu, J.F., Wang, Q., Wu, X.Y., 2004a. Crustal-mantle interaction during the thermo-tectonic reactivation of the North China Craton: SHRIMP zircon U-Pb age, petrology and geochemistry of Mesozoic plutons in western Shandong. Contributions to Mineralogy and Petrology 147, 750–767.

Xu, Y.G., Ma, J.L., Huang, X.L., Iizuka, Y., Chung, S.L., Wang, Y.B., Wu, X.Y., 2004b. Early Cretaceous gabbroic complex from Yinan, Shandong province: petrogenesis and mantle domains beneath the North China Craton. International Journal of Earth Sciences 93, 1025–1041.

Xu, W.L., Gao, S., Wang, Q.H., Wang, D.Y., Liu, Y.S., 2006a. Mesozoic crustal thickening of the eastern North China Craton: Evidence from eclogite xenoliths and petrologic implications. Geology 34, 721–724.

Xu, W.L., Wang, Q.H., Wang, D.Y., Guo, J.H., Pei, F.P., 2006b. Mesozoic adakitic rocks from the Xuzhou–Suzhou area, eastern China: evidence for partial melting of delaminated lower continental crust. Journal of Asian Earth Sciences 27, 230–240.

Xu, Y.G., Li, H.Y., Pang, C.J., He, B., 2009. On the timing and duration of the destruction of the North China Craton. Chinese Science Bulletin 54, 3379–3396.

Xu, Y.G., Zhang, H.H., Qiu, H.N., Ge, W.C., Wu, F.Y., 2012. Oceanic crust components in continental basalts from Shuangliao, Northeast China: Derived from the mantle transition zone? Chemical Geology 328, 168–184.

Yang, J.H., Wu, F.Y., 2009. Triassic magmatism and its relation to decratonization in the eastern North China Craton. Science in China Series D-Earth Sciences 52, 1319–1330.

Yang, J.H., Wu, F.Y., Wilde, S.A., 2003. Geodynamic setting of large-scale Late Mesozoic gold mineralization in the North China Craton: an association with lithospheric thinning. Ore Geology Reviews 23, 125–152.

Yang, J.H., Chung, S.L., Wilde, S.A., Wu, F.Y., Chu, M.F., Lo, C.H., Fan, H.R., 2005a. Petrogenesis of post-orogenic syenites in the Sulu Orogenic Belt, East China: geochronological, geochemical and Nd–Sr isotopic evidence. Chemical Geology 214, 99–125.

Yang, J.H., Wu, F.Y., Chung, S.L., Wilde, S.A., Chu, M.F., Lo, C.H., Song, B., 2005b. Petrogenesis of Early Cretaceous intrusions in the Sulu ultrahigh-pressure orogenic belt, east China and their relationship to lithospheric thinning. Chemical Geology 222, 200–231.

Yang, D.B., Xu, W.L., Pei, F.P., Yang, C.H., Wang, Q.H., 2012a. Spatial extent of the influence of the deeply subducted South China Block on the southeastern North China Block: Constraints from Sr–Nd–Pb isotopes in Mesozoic mafic igneous rocks. Lithos 136–139, 246–260.

Yang, Q.L., Zhao, Z.F., Zheng, Y.F., 2012b. Modification of subcontinental lithospheric mantle above continental subduction zone: Constraints from geochemistry of Mesozoic gabbroic rocks in southeastern North China. Lithos 146–147, 164–182.

Yu, S.Y., Xu, Y.G., Ma, J.L., Zheng, Y.F., Kuang, Y.S., Hong, L.B., Ge, W.C., Tong, L.X., 2010. Remnants of oceanic lower crust in the subcontinental lithospheric mantle: trace element and O isotope evidence from aluminous garnet pyroxenite xenoliths from Jiaohe, Northeast China. Earth and Planetary Science Letters 297, 413–422.

Zhai, M.G., Fan, Q.C., Zhan, H.F., Sui, J.L., Shao, J.A., 2007. Lower crustal processes leading to Mesozoic lithospheric thinning beneath eastern North China: Underplating, replacement and delamination. Lithos 96, 36–54.

Zhang, H.F., Gao, S., 2002. Geochemical and Sr–Nd–Pb isotopic compositions of Cretaceous granitoids: constraints on tectonic framework and crustal structure of the Dabieshan ultrahigh-pressure metamorphic belt, China. Chemical Geology 186, 281–299.

Zhang, T., Zhang, Y.Q., 2007. Geochronological sequence of Mesozoic intrusive magmatism in Jiaodong Peninsula and its tectonic constraints. Geological Journal of China Universities 13, 323–336 (in Chinese with English abstract).

Zhang, H.F., Sun, M., Zhou, X.H., Fan, W.M., Zhai, M.G., Yin, J.F., 2002. Mesozoic lithospheric destruction beneath the North China Carton: evidence from major-, trace-element and Sr–Nd–Pb isotope studies of Fangcheng basalts. Contributions to Mineralogy and Petrology 144, 241–253.

Zhang, H.F., Zhai, M.G., Tong, Y., Peng, P., Xu, B.L., Guo, J.H., 2006. Petrogenesis of the Sanfoshan High-Ba-Sr granite, Jiaodong Peninsula, eastern China. Geological Review 52, 43–53 (in Chinese with English abstract).

Zhang, J.J., Zheng, Y.F., Zhao, Z.F., 2009. Geochemical evidence for interaction between oceanic crust and lithospheric mantle in the origin of Cenozoic continental basalts in east-central China. Lithos 110, 305–326.

Zhang, C., Ma, C.Q., Holtz, F., 2010a. Origin of high-Mg adakitic magmatic enclaves from the Meichuan pluton, southern Dabie orogen (central China): Implications for delamination of the lower continental crust and melt-mantle interaction. Lithos 119, 467–484.

Zhang, J., Zhao, Z.F., Zheng, Y.F., Dai, M.N., 2010b. Postcollisional magmatism: geochemical constraints on the petrogenesis of Mesozoic granitoids in the Sulu orogen, China. Lithos 119, 512–536.

Zhang, C., Holtz, C., Ma, C.Q., Wolff, P.E., Li, X.Y., 2012. Tracing the evolution and distribution of F and Cl in plutonic systems from volatile-bearing minerals: a case study from the Liujiawa pluton (Dabie orogen, China). Contributions to Mineralogy and Petrology 164, 859–879.

Zhao, G.T., Cao, Q.C., Wang, D.Z., Li, H.M., 1997. Zirconic U-Pb dating on the Laoshan granitoids and its significance. Journal of Ocean University of Qingdao 27, 382–388 (in Chinese with English abstract).

Zhao, D., Lei, J., Tang, R., 2004. Origin of the Changbai intraplate volcano in Northeast China: evidence from seismic tomography. Chinese Science Bulletin 49, 1401–1408.

Zhao, G.C., Sun, M., Wilde, S.A., Li, S.Z., 2005. Late Archean to Paleoproterozoic evolution of the North China Craton: key issues revisited. Precambrian Research 136, 177–202.

Zheng, Y.F., Fu, B., Gong, B., Li, L., 2003. Stable isotope geochemistry of ultrahigh pressure metamorphic rocks from the Dabie–Sulu orogen in China: implications for geodynamics and fluid regime. Earth-Science Reviews 62, 105–161.

Zheng, J.P., Griffin, W.L., O'Reilly, S.Y., Yang, J.S., Zhang, R.Y., 2006. A refractory mantle protolith in younger continental crust, east-central China: Age and composition of zircon in the Sulu ultrahigh-pressure peridotite. Geology 34, 705–708.

Zheng, J.P., Griffin, W.L., O'Reilly, S.Y., Yu, C.M., Zhang, H.F., Pearson, N., Zhang, M., 2007. Mechanism and timing of lithospheric modification and replacement beneath the eastern North China Craton: peridotitic xenoliths from the 100 Ma Fuxin basalts and a regional synthesis. Geochimica et Cosmochimica Acta 269, 496–506.

Zhou, J.B., Zheng, Y.F., Zhao, Z.F., 2003. Zircon U-Pb dating on Mesozoic granitoids at Wulian, Shangdong province. Geological Journal of China Universities 9, 187–194 (in Chinese with English abstract).

Zhu, C., Sverjensky, D.A., 1991. Partitioning of F-Cl-OH between minerals and hydrothermal fluids. Geochimica et Cosmochimica Acta 55, 1837–1858.

Zhu, R.X., Xu, Y.G., Zhu, G., Zhang, H.F., Xia, Q.K., Zheng, T.Y., 2012a. Destruction of the North China Craton. Science in China Series D-Earth Sciences 55, 1565–1587.

Zhu, R.X., Yang, J.H., Wu, F.Y., 2012b. Timing of destruction of the North China Craton. Lithos 149, 51–60.